

Continual Learning: Forget-free Winning Subnetworks for Video Representations

Haeyong Kang, Jaehong Yoon, Sung Ju Hwang, and Chang D. Yoo*

Abstract—Inspired by the *Regularized Lottery Ticket Hypothesis (RLTH)*, which highlights the presence of competitive subnetworks within dense networks for continual learning tasks, we introduce *Winning Subnetworks (WSN)*. This approach utilizes reused weights in dense networks to enhance learning in Task Incremental Learning (TIL) scenarios. To mitigate overfitting in Few-Shot Class Incremental Learning (FSCIL), we have developed WSN variants referred to as the *Soft subnetwork (SoftNet)*. Furthermore, addressing WSN's limitation of sparse reused weights in Video Incremental Learning (VIL), we propose the *Fourier Subneural Operator (FSO)*. The FSO, operating in Fourier space, adaptively and compactly encodes videos, discovering reusable subnetworks with diverse bandwidths. We have applied FSO's Fourier representations to various continual learning contexts, including VIL, TIL, and FSCIL. Our extensive experiments across these scenarios demonstrate FSO's remarkable efficacy in continual learning, significantly enhancing task performance at various convolutional representational levels: it boosts performance in the higher layers for TIL and FSCIL and the lower layers for VIL.

Index Terms—Continual Learning (CL), Task Incremental Learning (TIL), Video Incremental Learning (VIL), Few-shot Class Incremental Learning (FSCIL), Regularized Lottery Ticket Hypothesis (RLTH), Winning SubNetworks (WSN), Soft-Subnetwork (SoftNet), Fourier Subneural Operator (FSO)

1 INTRODUCTION

CONTINUAL Learning (CL), also known as Lifelong Learning [82], [66], [96], [24], is a learning paradigm where a series of tasks are learned sequentially. The principle objective of continual learning is to replicate human cognition, characterized by the ability to learn new concepts or skills incrementally throughout one's lifespan. An optimal continual learning system could facilitate a positive forward and backward transfer, leveraging the knowledge gained from previous tasks to solve new ones while also updating its understanding of previous tasks with the new knowledge. However, building successful continual learning systems is challenging due to the occurrence of *catastrophic forgetting* or *catastrophic interference* [55], a phenomenon where the performance of the model on previous tasks significantly deteriorates when it learns new tasks. This can make it challenging to retain the knowledge acquired from previous tasks, ultimately leading to a decline in overall performance. To tackle the catastrophic forgetting problem in continual learning, numerous approaches have been proposed, which can be broadly classified as follows: (1) Regularization-based methods [37], [4], [31], [83], [59] aim to keep the learned information of past tasks during continual training aided by sophisticatedly designed regularization terms, (2) Rehearsal-based methods [64], [65], [5], [6], [67], [68] utilize a set of real or synthesized data from the previous tasks and revisit them, and (3) Architecture-based methods [52], [70], [44], [89], [33], [34] propose to minimize the inter-task interference via newly designed architectural components.

Despite the remarkable success of recent works on rehearsal- and architecture-based continual learning, most

current methods request external memory as new tasks arrive, making the model difficult to scale to larger and more complex tasks. Rehearsal-based CL requires additional storage to store the replay buffer or generative models, and architecture-based methods leverage additional model capacity to account for new tasks. These trends lead to an essential question: how can we build a memory-efficient CL model that does not exceed the backbone network's capacity or even requires a much smaller capacity? Several studies have shown that deep neural networks are over-parameterized [18], [23], [43] and thus removing redundant/unnecessary weights can achieve on-par or even better performance than the original dense network. More recently, Lottery Ticket Hypothesis (LTH) [20] demonstrates the existence of sparse subnetworks, named *winning tickets*, that preserve the performance of a dense network. However, searching for optimal winning tickets during continual learning with iterative pruning methods requires repetitive pruning and retraining for each arriving task, which could be more practical.

To tackle the issues of external replay buffer, capacity, and over-fitting, we suggest a novel CL method, which finds the high-performing *Winning SubNetwork* referred to as WSN [33] given tasks without the need for retraining and rewinding, as shown in Figure 1 (d). Also, we set previous pruning-based CL approaches [52], [89] (see Figure 1 (a)) to baselines of architectures, which obtain task-specific subnetworks given a pre-trained backbone network. Our WSN incrementally learns model weights and task-adaptive binary masks (the subnetworks) within the neural network. To allow the forward transfer when a model learns on a new task, we reuse the learned subnetwork weights for the previous tasks, however selectively, as opposed to using all the weights [53] (see Figure 1 (b)), that may lead to

Email: haeyong.kang@kaist.ac.kr

* Corresponding Author.

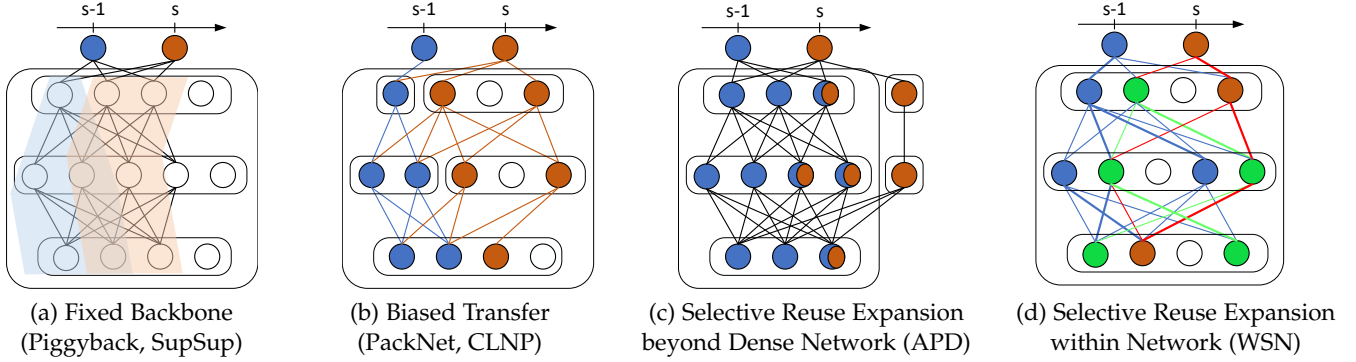


Fig. 1: **Concept Comparison:** (a) Piggyback [52], and SupSup [89] find the optimal binary mask on a fixed backbone network a given task (b) PackNet [53] and CLNP [21] forces the model to reuse all features and weights from previous subnetworks which cause bias in the transfer of knowledge (c) APD [93] selectively reuse and dynamically expand the dense network (d) Our WSN selectively reuse and dynamically expand subnetworks within a dense network. **Green edges** are reused weights.

biased transfer. Further, the WSN eliminates the threat of catastrophic forgetting during continual learning by freezing the subnetwork weights for the previous tasks and does not suffer from the negative transfer, unlike [95] (see Figure 1 (c)), whose subnetwork weights for the previous tasks can be updated when training on the new sessions. Moreover, we observed that subnetworks could overfit to limited task data, potentially reducing their effectiveness on new tasks or datasets, such as in Few-Shot Class Incremental Learning (FSCIL). To address this, we adopted the Regularized Lottery Ticket Hypothesis (RLTH) [34]. This led to the discovery of regularized subnetworks characterized by smoother (soft) masks referred to as Soft-SubNetwork (SoftNet), enhancing their adaptability and performance.

While these conventional architecture-based methods, i.e., WSN and SoftNet, offer solutions to prevent forgetting, they are unsuited for sequential complex Video Continual Learning (VCL) as they reuse a few or all adaptive parameters without finely discretized operations. To enhance neural representation incrementally on complex sequential videos, we propose a novel sequential video compilation method to identify and utilize Lottery tickets (i.e., the weights of complicated oscillatory signals) in frequency space. To achieve this, we define Fourier Subnetwork Operator (FSO), which breaks down a neural implicit representation into its sine and cosine components (real and imaginary parts) and then selectively identifies the most effective *Lottery tickets* for representing complex periodic signals. In practice, given a backbone and FSO architecture, our method continuously learns to identify input-adaptive subnetwork modules and encode each new video into the corresponding module during sequential training sessions. We extend Fourier representations to various continual learning scenarios, such as Task Incremental Learning (TIL), Video Incremental Learning (VIL), and Few-shot Class Incremental Learning (FSCIL), to demonstrate the effectiveness of FSO.

Our contributions can be summarized as follows:

- We introduce Fourier Subnetwork Operator (FSO), which breaks down a neural implicit representation into its sine and cosine components (real and imaginary parts) and then selectively identifies the most effective *Lottery tickets* for representing complex periodic signals such as sequential video compilation.
- We have expanded the FSO of Fourier representations to

encompass a variety of continual learning scenarios: Video Incremental Learning (VIL), Task Incremental Learning (TIL), and Few-Shot Class Incremental Learning (FSCIL). In our evaluations, the proposed FSO demonstrates superior performance compared to architecture-based continual learning models, such as WSN and SoftNet in TIL, VIL, and FSCIL, respectively, thereby underscoring its exceptional representational power.

2 RELATED WORKS

Continual Learning [55], [82], [41], [45], also known as lifelong learning, is the challenge of learning a sequence of tasks continuously while utilizing and preserving previously learned knowledge to improve performance on new tasks. Four major approaches have been proposed to tackle the challenges of continual learning, such as catastrophic forgetting. One such approach is *regularization-based methods* [37], [4], [31], [83], [59], which aim to reduce catastrophic forgetting by imposing regularization constraints that inhibit changes to the weights or nodes associated with past tasks. *Rehearsal-based approaches* [64], [5], [6], [67], [17], [79], [68] store small data summaries to the past tasks and replay them during training to retain the acquired knowledge. Some methods in this line of work [73], [2] accommodate the generative model to construct the pseudo-rehearsals for previous tasks. *Architecture-based approaches* [52], [70], [44], [89], [33], [34] use the additional capacity to expand [91], [95], dynamic representation [92], [74] or isolate [66] model parameters, preserving learned knowledge and preventing forgetting. Both rehearsal and architecture-based methods have shown remarkable efficacy in suppressing catastrophic forgetting but require additional capacity for the task-adaptive parameters [89] or the replay buffers. *Prompt-based learning*, an emerging transfer learning technique in the field of natural language processing (NLP), harnesses a fixed function to condition the model. This empowers the language model to receive additional instructions for enhancing its performance on downstream tasks. Notably, while L2P [88] stands out as the seminal work that bridges the gap between prompting and continual learning, DualPrompt [87] introduces an innovative approach to affixing complementary prompts to the pre-trained backbone, thereby enabling the acquisition of both task-invariant and task-specific instructions. Additionally, other notable contributions in this field encompass

DyTox [19], S-Prompt [86], CODA-P [77], ConStruct-VL [76], ST-Prompt [61], and LGCL [35]. Nonetheless, the central focus of this study is to pinpoint the most optimal winning tickets for convolutional operators in a wide array of continual learning scenarios, both in real and Fourier space.

Architecture-based Continual Learning. While most works aim to increase the performance of continual learners by adding memory, some researchers have focused on building memory and computationally efficient continual learners by using pruning-based constraints. CLNP [21] is one example of a method that selects important neurons for a given task using ℓ_1 regularization to induce sparsity and freezes them to maintain performance. Neurons that are not selected are reinitialized for future task training. Another method, Piggyback [52], trains task-specific binary masks on the weights given a pre-trained model. However, this method does not allow for knowledge transfer among tasks, and its performance highly depends on the quality of the backbone model. HAT [70] proposes task-specific learnable attention vectors to identify important weights per task. The masks are formulated to layerwise cumulative attention vectors during continual learning. A recent method, LL-Tickets [12], shows a sparse subnetwork called lifelong tickets that performs well on all tasks during continual learning. The method searches for more prominent tickets from current ones if the obtained tickets cannot sufficiently learn the new task while maintaining performance on past tasks. However, LL-Tickets require external data to maximize knowledge distillation with learned models for prior tasks, and the ticket expansion process involves retraining and pruning steps. WSN [33] is another method that jointly learns the model and task-adaptive binary masks on subnetworks associated with each task. It attempts to select a small set of weights activated (winning ticket) by reusing weights of the prior subnetworks in Task Incremental Learning (TIL). We also investigate the performance of Soft-Subnetworks (SoftNet) [34]. We select sub-networks (winning tickets) to obtain base session knowledge and optimize the regularized sub-network parameters for new sessions in Few-Shot Class Incremental Learning (FSCIL) settings.

Neural Implicit Representation (NIR) [56] are neural network architectures for parameterizing continuous, differentiable signals. Based on coordinate information, they provide a way to represent complex, high-dimensional data with a small set of learnable parameters that can be used for various tasks such as image reconstruction [75], [80], shape regression [13], [60], and 3D view synthesis [58], [69]. Instead of using coordinate-based methods, NeRV [10] proposes an image-wise implicit representation that takes frame indices as inputs, enabling fast and accurate video compression. NeRV has inspired further improvements in video regression by CNeRV [8], DNeRV [25], E-NeRV [46], and NIRVANA [51], and HNeRV [9]. A few recent works have explored video continual learning (VCL) scenarios for the NIR. To tackle non-physical environments, Continual Predictive Learning (CPL) [7] learns a mixture world model via predictive experience replay and performs test-time adaptation using non-parametric task inference. PIVOT [85] leverages the past knowledge present in pre-trained models from the image domain to reduce the number of trainable parameters and mitigate forgetting. CPL needs memory

to replay, while PIVOT needs pre-training and fine-tuning steps. In contrast, along with the conventional progressive training techniques [66], [16], we use WSN as baselines, which utilizes the Lottery Ticket Hypothesis (LTH) to identify an adaptive substructure within the dense networks that are tailored to the specific video input index. However, WSN is inappropriate for sequential complex video compilation since it reuses a few adaptive but sparse learnable parameters. To overcome the weakness of WSN, We proposed a novel Fourier Subneural Operator (FSO) for representing complex video in Fourier space [47], [48], [38], [84]. We have expanded the FSO of Fourier representations to encompass a variety of continual learning architectures and scenarios to validate its effectiveness.

3 WINNING SUBNETWORKS IN FOURIER SPACE

In this section, we present our pruning-based continual learning methods, *Winning SubNetworks* (WSN, see Figure 2) [33]. The WSN searches for the task-adaptive winning tickets and updates only the weights that have not been trained on the previous tasks, as shown in Figure 2. After training on each session, the subnetwork parameters of the model are frozen to ensure that the proposed method is inherently immune to catastrophic forgetting. Moreover, we illustrate *Soft-Winning SubNetworks* (SoftNet) [34], proposed to address the issues of forgetting previous sessions and overfitting a few samples of new sessions. These conventional architecture-based methods, i.e., WSN and SoftNet, offer solutions to prevent forgetting, however, they are unsuited for sequential complex Video Incremental Learning (VIL see Figure 3) as they reuse a few or all adaptive parameters without finely discretized operations. To enhance neural representation incrementally on complex sequential videos, we introduce Fourier Subnetwork Operator (FSO), which breaks down a neural implicit representation into its sine and cosine components (real and imaginary parts) and then selectively identifies the most effective *Lottery tickets* for representing complex periodic signals. In practice, given a backbone and FSO architecture, our method continuously learns to identify input-adaptive subnetwork modules and encode each new video into the corresponding module during sequential training sessions. We extend Fourier representations to various continual learning scenarios, such as TIL, VIL, and FSCIL, to demonstrate the effectiveness of FSO.

Problem Statement. Consider a supervised learning setup where S sessions or tasks arrive to a learner sequentially. We denote that $\mathcal{D}_s = \{\mathbf{x}_{i,s}, y_{i,s}\}_{i=1}^{n_s}$ is the dataset of session s , composed of n_s pairs of raw instances and corresponding labels. We assume a neural network $f(\cdot; \theta)$, parameterized by the model weights θ and standard continual learning scenario aims to learn a sequence of sessions by solving the following optimization procedure at each step s :

$$\theta^* = \underset{\theta}{\text{minimize}} \frac{1}{n_s} \sum_{i=1}^{n_s} \mathcal{L}(f(\mathbf{x}_{i,s}; \theta), y_{i,s}), \quad (1)$$

where $\mathcal{L}(\cdot, \cdot)$ is a classification objective loss such as cross-entropy loss. \mathcal{D}_s for session s is only accessible when learning session s .

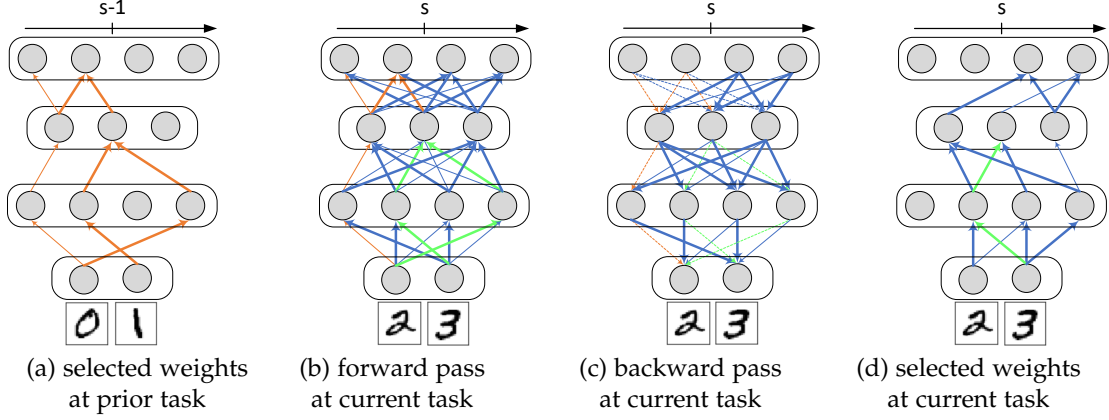


Fig. 2: **An illustration of Winning SubNetworks (WSN):** (a) The top- $c\%$ weights $\hat{\theta}_{s-1}$ at prior task are obtained, (b) In the forward pass of a new task, WSN reuses weights selected from prior tasks, (c) In the backward pass, WSN updates only non-used weights, and (d) after several iterations of (b) and (c), we acquire again the top- $c\%$ weights $\hat{\theta}_s$ including subsets of **reused weights (green)** for the new task.

Continual learners frequently use over-parameterized deep neural networks to ensure enough capacity for learning future tasks. This approach often leads to the discovery of subnetworks that perform as well as or better than the dense network. Given the neural network parameters θ , the binary attention mask m_s^* that describes the optimal subnetwork for session s such that $|m_s^*|$ is less than the model capacity c follows as:

$$m_s^* = \underset{m_s \in \{0,1\}^{|\theta|}}{\text{minimize}} \frac{1}{n_s} \sum_{i=1}^{n_s} \mathcal{L}(f(\mathbf{x}_{i,s}; \theta \odot m_s), y_{i,s}) - \mathcal{J} \quad (2)$$

subject to $|m_s^*| \leq c$,

where session loss $\mathcal{J} = \mathcal{L}(f(\mathbf{x}_{i,s}; \theta), y_{i,s})$ and $c \ll |\theta|$ (used as the selected proportion % of model parameters in the following section). In the optimization section, we describe how to obtain m_t^* using a single learnable weight score ρ that is subject to updates while minimizing session loss jointly for each task or session.

3.1 Fourier Subneural Operator (FSO)

Conventional continual learner (i.e., WSN) only uses a few learnable parameters in convolutional operations to represent complex sequential image streams in Video Incremental Learning. To capture more parameter-efficient and forget-free video representations (i.e., Neural Implicit Representation (NIR), see Figure 3), the NIR model requires fine discretization and video-specific sub-parameters. This motivation leads us to propose a novel subnetwork operator in Fourier space, which provides it with various bandwidths. Following the previous definition of Fourier convolutional operator [47], we adapt and redefine this definition to better fit the needs of the NIR framework. We use the symbol \mathcal{F} to represent the Fourier transform of a function f , which maps from an embedding space of dimension $d_e = 1 \times 160$ to a frame size denoted as d_v . The inverse of this transformation is represented by \mathcal{F}^{-1} . In this context, we introduce our Fourier-integral Subneural Operator (FSO), symbolized as \mathcal{K} , which is tailored to enhance the capabilities of our NIR system:

$$(\mathcal{K}(\phi)e_{s,t})(v_t^s) = \mathcal{F}^{-1}(R_\phi \cdot (\mathcal{F}e_{s,t}))(v_t^s), \quad (3)$$

where R_ϕ is the Fourier transform of a periodic subnetwork function which is parameterized by its subnetwork's param-

eters of real ($\theta^{real} \odot m_s^{real}$) and imaginary ($\theta^{imag} \odot m_s^{imag}$). We thus parameterize R_ϕ separately as complex-valued tensors of real and imaginary $\phi_{FSO} \in \{\theta^{real}, \theta^{imag}\}$. One key aspect of the FSO is that its parameters grow with the depth of the layer and the input/output size. However, through careful layer-wise inspection and adjustments for sparsity, we can find a balance that allows the FSO to describe neural implicit representations efficiently. In the experimental section, we will showcase the most efficient FSO structure and its performance. Figure 3 shows one possible structure of a single FSO. We describe the optimization in the following section.

For Task/Class Incremental Learnings, Convolutional Neural Networks (CNNs) take a convolutional operation, followed by a pooling operation. These iterative operations of CNNs represent more abstract features at higher layer output levels and lose global contextual representations. To compensate for low-contextual representations, we add an FSO to CNN architecture as shown in Figure 4. The lower layer's output x^{l-1} is merged into the l th layer residual block through the FSO to acquire spatially ensembling features x^l . The FSO also provides additional parameters to push the residual to zero. We show the differences between ensembling features (WSN+FSO) and single features (WSN) represented by residual blocks as shown in Figure 5: WSN+FSO provides lower variances of feature maps and higher frequency components than WSN. In the following experimental settings, we investigate various CNN architectures with FSO.

3.2 SubNetworks with FSO

3.2.1 Winning SubNetworks (WSN) with FSO

Let each weight $\theta_* = \{\theta, \phi_{FSO}\}$ be associated with a learnable parameter we call *weight score* $\rho_* = \{\rho, \rho_{FSO}\}$, which numerically determines the importance of the weight associated with it; that is, a weight with a higher weight score is seen as more important. We find a sparse subnetwork θ_s of the neural network and assign it as a solver of the current session s . We use subnetworks instead of the dense network as solvers for two reasons: (1) Lottery Ticket Hypothesis [20] shows the existence of a subnetwork that performs as well as the whole network, and (2) subnetwork requires less capacity

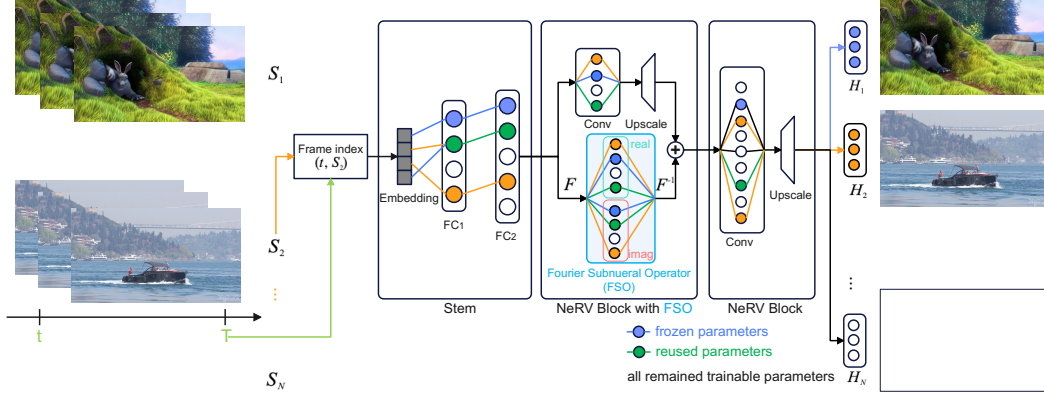


Fig. 3: **Forget-free Neural Implicit Representation with Fourier Subneural Operator (FSO) for Video Incremental Learning:** Image-wise neural implicit representation taking frame and video (session s) indices as input and using a sparse Stems + NeRV Blocks with *Fourier Subneural Operator* (FSO) to output the whole image through multi-heads H_N . We denote frozen, reused, and trainable parameters in training at session 2. Note that each video representation is colored. In inference, we only need indices of session s and frame t and session mask (subnetwork).

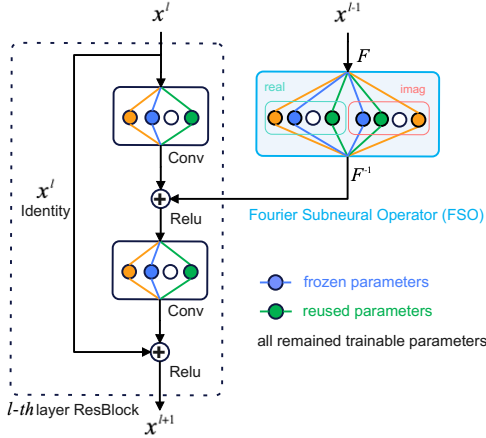


Fig. 4: **Residual Blocks (ResBlocks) with Fourier Subneural Operator (FSO).**

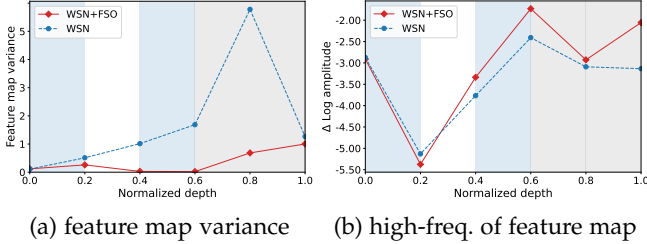


Fig. 5: **The comparisons of WSN of 4 Conv (blue area) and 3 FC (gray area) with FSO (white area) in terms of Feature variances and high-frequency components:** the (a) offers the variance of the feature map and the (b) provides $\Delta \log$ amplitudes at high-frequency (1.0π).

than dense networks, and therefore it inherently reduces the size of the expansion of the solver.

Motivated by such benefits, we propose a novel *Winning SubNetworks* (WSN¹), which is the joint-training method for continual learning that trains on session - while selecting an important subnetwork given the session s as shown in Fig. 2. The illustration of WSN explains step-by-step how to acquire binary weights within a dense network. We find $\hat{\theta}_t$ by selecting the $c\%$ weights with the highest weight scores ρ_* , where c is the target layerwise capacity ratio in %. A task-

dependent binary weight represents the selection of weights \mathbf{m}_s where a value of 1 denotes that the weight is selected during the forward pass and 0 otherwise. Formally, \mathbf{m}_s is obtained by applying a indicator function $\mathbb{1}_c$ on ρ where $\mathbb{1}_c(\rho) = 1$ if ρ_* belongs to top- $c\%$ scores and 0 otherwise. Therefore, the subnetwork $\hat{\theta}_s$ for session s is obtained by $\hat{\theta}_s = \theta_* \odot \mathbf{m}_s$.

3.2.2 Soft-Subnetworks (SoftNet) with FSO

Several works have addressed overfitting issues in continual learning from different perspectives, including NCM [30], BiC [90], OCS [94], and FSLL [54]. To mitigate the overfitting issue in subnetworks, we use a simple yet efficient method named *SoftNet* proposed by [34]. The following new paradigm, referred to as *Regularized Lottery Ticket Hypothesis* [34] which is inspired by the *Lottery Ticket Hypothesis* [20] has become the cornerstone of SoftNet:

Regularized Lottery Ticket Hypothesis (RLTH). *A randomly-initialized dense neural network contains a regularized subnetwork that can retain the prior class knowledge while providing room to learn the new class knowledge through isolated training of the subnetwork.*

Based on RLTH, we propose a method, referred to as *Soft-SubNetworks* (SoftNet²). SoftNet jointly learns the randomly initialized dense model, and soft mask $\mathbf{m} \in [0, 1]^{|\theta_*|}$ on Soft-subnetwork on each session training; the soft mask consists of the major part of the model parameters $m = 1$ and the minor ones $m < 1$ where $m = 1$ is obtained by the top- $c\%$ of model parameters and $m < 1$ is obtained by the remaining ones ($100 - \text{top-}c\%$) sampled from the uniform distribution $U(0, 1)$. Here, it is critical to select minor parameters $m < 1$ in a given dense network.

3.3 Optimization for TIL, VIL, and FSCIL

3.3.1 Winning SubNetworks (WSN) for TIL

To jointly learn the model weights and task-adaptive binary masks of subnetworks associated with each session, given

1. WSN code is available at <https://github.com/ihaeyong/WSN.git>

2. SoftNet code is available at <https://github.com/ihaeyong/SoftNet-FSCIL.git>

an objective $\mathcal{L}(\cdot)$, i.e., cross-entropy loss, we optimize θ_* and ρ_* with:

$$\underset{\theta_*, \rho_*}{\text{minimize}} \mathcal{L}(\theta_* \odot \mathbf{m}_s; \mathcal{D}_s). \quad (4)$$

However, this vanilla optimization procedure presents two problems: (1) updating all θ_* when training for new sessions will cause interference to the weights allocated for previous sessions, and (2) the indicator function always has a gradient value of 0; therefore, updating the weight scores ρ_* with its loss gradient is not possible. To solve the first problem, we selectively update the weights by allowing updates only on the weights not selected in the previous sessions. To do that, we use an *accumulate binary mask* $\mathbf{M}_{s-1} = \bigvee_{i=1}^{s-1} \mathbf{m}_i$ when learning session s , then for an optimizer with learning rate η , the θ_* is updated as follows:

$$\theta_* \leftarrow \theta_* - \eta \left(\frac{\partial \mathcal{L}}{\partial \theta_*} \odot (\mathbf{1} - \mathbf{M}_{s-1}) \right), \quad (5)$$

effectively freezing the weights of the subnetworks selected for the previous sessions. To solve the second problem, we use Straight-through Estimator [29], [3], [63] in the backward pass since \mathbf{m}_s is obtained by top- $c\%$ scores. Specifically, we ignore the derivatives of the indicator function and update the weight score as follows:

$$\rho_* \leftarrow \rho_* - \eta \left(\frac{\partial \mathcal{L}}{\partial \rho_*} \right). \quad (6)$$

Our WSN optimizing procedure is summarized in Algorithm 1.

Algorithm 1 Winning SubNetworks (WSN) for TIL and VIL.

input $\{\mathcal{D}_s\}_{s=1}^S$, model weights $\theta_* = \{\theta, \phi_{FSO}\}$, score weights $\rho_* = \{\rho, \rho_{FSO}\}$, binary mask $\mathbf{M}_0 = \{\mathbf{0}^{|\theta|}, \mathbf{0}^{|\theta_{FSO}|}\}$, layer-wise capacity $c\%$.

- 1: Randomly initialize θ_* and ρ_* .
- 2: **for** task $s = 1, \dots, S$ **do**
- 3: **for** batch $\mathbf{b}_s \sim \mathcal{D}_s$ **do**
- 4: Obtain mask \mathbf{m}_s of the top- $c\%$ scores ρ_*
- 5: Compute $\mathcal{L}(\theta_* \odot \mathbf{m}_s; \mathbf{b}_s)$
- 6: $\theta_* \leftarrow \theta_* - \eta \left(\frac{\partial \mathcal{L}}{\partial \theta_*} \odot (\mathbf{1} - \mathbf{M}_{s-1}) \right)$ ▷ Weight update
- 7: $\rho_* \leftarrow \rho_* - \eta \left(\frac{\partial \mathcal{L}}{\partial \rho_*} \right)$ ▷ Weight score update
- 8: **end for**
- 9: $\mathbf{M}_s \leftarrow \mathbf{M}_{s-1} \vee \mathbf{m}_s$ ▷ Accumulate binary mask
- 10: **end for**

3.3.2 Winning SubNetworks (WSN) for VIL

Let a video at s_{th} session $\mathbf{V}_s = \{\mathbf{v}_t^s\}_{t=1}^{T_s} \in \mathbb{R}^{T_s \times H \times W \times 3}$ be represented by a function with the trainable parameter θ_* , $f_{\theta_*} : \mathbb{R} \rightarrow \mathbb{R}^{H \times W \times 3}$, during Video Incremental Learning (VIL), where T_s denotes the number of frames in a video at session s , and $s \in \{1, \dots, |S|\}$. Given a session and frame index s and t , respectively, the neural implicit representation aims to predict a corresponding RGB image $\mathbf{v}_t^s \in \mathbb{R}^{H \times W \times 3}$ by fitting an encoding function to a neural network: $\mathbf{v}_t^s = f_{\theta_*}([s; t], H_s)$ where H_s is s_{th} head. For the sake of simplicity, we omit H_s in the following equations. Let's consider a real-world learning scenario in which $|S| = N$ or more sessions arrive in the model sequentially. We denote that $\mathcal{D}_s = \{\mathbf{e}_{s,t}, \mathbf{v}_{s,t}\}_{t=1}^{T_s}$ is the dataset of session s , composed of T_s pairs of raw embeddings $\mathbf{e}_{s,t} = [\mathbf{e}_s; \mathbf{e}_t] \in \mathbb{R}^{1 \times 160}$

and corresponding frames \mathbf{v}_t^s . Here, we assume that \mathcal{D}_s for session s is only accessible when learning session s due to the limited hardware memory and privacy-preserving issues, and session identity is given in the training and testing stages. The primary training objective in this sequence of N video sessions is to minimize the following optimization problem:

$$\underset{\theta_*, \rho_*}{\text{minimize}} \frac{1}{N} \frac{1}{T_s} \sum_{s=1}^N \sum_{t=1}^{T_s} \mathcal{L}(f(\mathbf{e}_{s,t}; \theta_* \odot \mathbf{m}_s), \mathbf{v}_t^s), \quad (7)$$

where the loss function $\mathcal{L}(\mathbf{v}_t^s)$ is composed of ℓ_1 loss and SSIM loss. The former minimizes the pixel-wise RGB gap with the original input frames evenly, and the latter maximizes the similarity between the two entire frames based on luminance, contrast, and structure, as follows:

$$\mathcal{L}(\mathbf{V}_s) = \frac{1}{T_s} \sum_{t=1}^{T_s} \alpha \|\mathbf{v}_t^s - \hat{\mathbf{v}}_t^s\|_1 + (1-\alpha)(1-\text{SSIM}(\mathbf{v}_t^s, \hat{\mathbf{v}}_t^s)), \quad (8)$$

where $\hat{\mathbf{v}}_t^s$ is the output generated by the model f . For all experiments, we set the hyperparameter α to 0.7, and we adapt PixelShuffle [72] for session and time positional embedding.

3.3.3 Soft-SubNetworks (SoftNet) for FSCIL

Similar to WSN's optimization discussed in Section 3.3, let each weight θ_* be associated with a learnable parameter we call *weight score* ρ_* , which numerically determines the importance of the associated weight. In the optimization process for FSCIL, however, we consider two main problems: (1) Catastrophic forgetting: updating all $\theta_* \odot \mathbf{m}_{s-1}$ when training for new sessions will cause interference with the weights allocated for previous sessions; thus, we need to freeze all previously learned parameters $\theta_* \odot \mathbf{m}_{s-1}$; (2) Overfitting: the subnetwork also encounters overfitting issues when training an incremental session on a few samples, as such, we need to update a few parameters irrelevant to previous session knowledge, i.e., $\theta_* \odot (\mathbf{1} - \mathbf{m}_{s-1})$.

To acquire the optimal subnetworks that alleviate the two issues, we define a soft-subnetwork by dividing the dense neural network into two parts—one is the major subnetwork $\mathbf{m}_{\text{major}}$, and another is the minor subnetwork $\mathbf{m}_{\text{minor}}$. The defined Soft-SubNetwork (SoftNet) follows as:

$$\mathbf{m}_{\text{soft}} = \mathbf{m}_{\text{major}} \oplus \mathbf{m}_{\text{minor}}, \quad (9)$$

where $\mathbf{m}_{\text{major}}$ is a binary mask and $\mathbf{m}_{\text{minor}} \sim U(0, 1)$ and \oplus represents an element-wise summation. As such, a soft-mask is given as $\mathbf{m}_s^* \in [0, 1]^{|\theta_*|}$. In the all-experimental FSCIL setting, $\mathbf{m}_{\text{major}}$ maintains the base session knowledge $s = 1$ while $\mathbf{m}_{\text{minor}}$ acquires the novel session knowledge $s \geq 2$. Then, with base session learning rate α , the θ_* is updated as follows: $\theta_* \leftarrow \theta_* - \alpha \left(\frac{\partial \mathcal{L}}{\partial \theta_*} \odot \mathbf{m}_{\text{soft}} \right)$ effectively regularize the weights of the subnetworks for incremental learning. Our Soft-subnetwork optimizing procedure is summarized in Algorithm 2. Once a single soft-subnetwork \mathbf{m}_{soft} is obtained in the base session, then we use the soft-subnetwork for the entire new sessions without updating.

Base Training ($s = 1$). In the base learning session, we optimize the soft-subnetwork parameter θ_* (including a fully connected layer as a classifier) and weight score ρ_*

Algorithm 2 Soft-Subnetworks (SoftNet) for FSCIL.

```

input  $\{\mathcal{D}^t\}_{t=1}^T$ , model weights  $\theta_* = \{\theta, \phi_{FSO}\}$ , and score
weights  $\rho_* = \{\rho, \rho_{FSO}\}$ , layer-wise capacity  $c$ 
1: // Training over base classes  $s = 1$ 
2: Randomly initialize  $\theta_*$  and  $\rho_*$ .
3: for epoch  $e = 1, 2, \dots$  do
4:   Obtain softmax  $\mathbf{m}_{\text{soft}}$  of  $\mathbf{m}_{\text{major}}$  and  $\mathbf{m}_{\text{minor}} \sim U(0, 1)$ 
   at each layer
5:   for batch  $\mathbf{b}_s \sim \mathcal{D}^s$  do
6:     Compute  $\mathcal{L}_{\text{base}}(\theta_* \odot \mathbf{m}_{\text{soft}}; \mathbf{b}_s)$  by Equation 4
7:      $\theta_* \leftarrow \theta_* - \alpha \left( \frac{\partial \mathcal{L}}{\partial \theta_*} \odot \mathbf{m}_{\text{soft}} \right)$ 
8:      $\rho_* \leftarrow \rho_* - \alpha \left( \frac{\partial \mathcal{L}}{\partial \rho_*} \odot \mathbf{m}_{\text{soft}} \right)$ 
9:   end for
10: end for
11: // Incremental learning  $s \geq 2$ 
12: Combine the training data  $\mathcal{D}^s$ 
13:   and the exemplars saved in previous few-shot sessions
14: for epoch  $e = 1, 2, \dots$  do
15:   for batch  $\mathbf{b}_s \sim \mathcal{D}^s$  do
16:     Compute  $\mathcal{L}_m(\theta_* \odot \mathbf{m}_{\text{soft}}; \mathbf{b}_s)$  by Equation 10
17:      $\theta_* \leftarrow \theta_* - \beta \left( \frac{\partial \mathcal{L}}{\partial \theta_*} \odot \mathbf{m}_{\text{minor}} \right)$ 
18:   end for
19: end for
output model parameters  $\theta_*, \rho_*$ , and  $\mathbf{m}_{\text{soft}}$ .

```

with cross-entropy loss jointly using the training examples of \mathcal{D}^1 .

Incremental Training ($s \geq 2$). In the incremental few-shot learning sessions ($s \geq 2$), leveraged by $\theta_* \odot \mathbf{m}_{\text{soft}}$, we fine-tune few minor parameters $\theta_* \odot \mathbf{m}_{\text{minor}}$ of the soft-subnetwork to learn new classes. Since $\mathbf{m}_{\text{minor}} < \mathbf{1}$, the soft-subnetwork alleviates the overfitting of a few samples. Furthermore, instead of Euclidean distance [71], we employ a metric-based classification algorithm with cosine distance to finetune the few selected parameters. In some cases, Euclidean distance fails to give the real distances between representations, especially when two points with the same distance from prototypes do not fall in the same class. In contrast, representations with a low cosine distance are located in the same direction from the origin, providing a normalized informative measurement. We define the loss function as:

$$\mathcal{L}_m(\mathbf{x}, y; \theta_* \odot \mathbf{m}_{\text{soft}}) = - \sum_{\mathbf{x}, y \in \mathcal{D}} \sum_{o \in \mathcal{O}} \mathbb{1}(y = o) \log \left(\frac{e^{-d(\mathbf{p}_o, f(\mathbf{x}; \theta_* \odot \mathbf{m}_{\text{soft}}))}}{\sum_{o_k \in \mathcal{O}} e^{-d(\mathbf{p}_{o_k}, f(\mathbf{x}; \theta_* \odot \mathbf{m}_{\text{soft}}))}} \right) \quad (10)$$

where $d(\cdot, \cdot)$ denotes cosine distance, \mathbf{p}_o is the prototype of class o , $\mathcal{O} = \bigcup_{i=1}^s \mathcal{O}^i$ refers to all encountered classes, and $\mathcal{D} = \mathcal{D}^s \cup \mathcal{P}$ denotes the union of the current training data \mathcal{D}^s and the exemplar set $\mathcal{P} = \{\mathbf{p}_2 \dots, \mathbf{p}_{s-1}\}$, where \mathcal{P}_{s_e} ($2 \leq s_e < s$) is the set of saved exemplars in session s_e . Note that the prototypes of new classes are computed by $\mathbf{p}_o = \frac{1}{N_o} \sum_i \mathbb{1}(y_i = o) f(\mathbf{x}_i; \theta_* \odot \mathbf{m}_{\text{soft}})$ and those of base classes are saved in the base session, and N_o denotes the number of the training images of class o . We also save the prototypes of all classes in \mathcal{O}^s for later evaluation.

Inference for Incremental Soft-Subnetwork. In each session, the inference is also conducted by a simple nearest class

mean (NCM) classification algorithm [57], [71] for fair comparisons. Specifically, all the training and test samples are mapped to the embedding space of the feature extractor f , and Euclidean distance $d_u(\cdot, \cdot)$ is used to measure their similarity. The classifier gives the k th prototype index $o_k^* = \arg \min_{o \in \mathcal{O}} d_u(f(\mathbf{x}; \theta_* \odot \mathbf{m}_{\text{soft}}), \mathbf{p}_o)$ as output.

4 EXPERIMENTS

We validate our method on several benchmark datasets against relevant continual learning baselines on Task-Incremental Learning (TIL), Video Incremental Learning (VIL), and Few-shot Class Incremental Learning (FSCIL).

4.1 Task-incremental Learning (TIL)

Datasets and architectures. We use three different popular sequential datasets for CL problems with three different neural network architectures as follows: 1) CIFAR-100 Split [39]: A visual object dataset constructed by randomly dividing 100 classes of CIFAR-100 into ten tasks with ten classes per task. 2) CIFAR-100 Superclass: We follow the setting from [93] that divides CIFAR-100 dataset into 20 tasks according to the 20 superclasses, and each superclass contains five different but semantically related classes. 3) TinyImageNet [78]: A variant of ImageNet [40] containing 40 of 5-way classification tasks with the image size by $64 \times 64 \times 3$.

We use variants of LeNet [42] for the experiments on CIFAR-100 Superclass experiments, and a modified version of AlexNet similar to [70], [67] for the CIFAR-100 Split dataset. For TinyImageNet, we also use the same network architecture as [22], [17], which consists of 4 Conv layers and 3 fully connected layers. We set WSN as the architecture-based baselines, which jointly train and find task-adaptive subnetworks of novel/prior parameters for continual learning. WSN+FSO follows the Residual Blocks as stated in Figure 4 in all three architectures. The FSO's ensemble structures follow in terms of three architectures:

- In the LeNet, the Conv. layer's output $\mathbf{x}^{l=1}$ is merged into the $l = 2$ th Conv. layer output through the FSO to acquire spatially ensembling features $\mathbf{x}^{l=2}$.
- In the AlexNet, the Conv. layer's output $\mathbf{x}^{l=2}$ is merged into the $l = 3$ th Conv. layer's output through the FSO to acquire spatially ensembling features $\mathbf{x}^{l=3}$.
- In the TinyImageNet, the Conv. layer's output $\mathbf{x}^{l=2}$ is merged into the $l = 3$ th Conv. layer's output through the FSO to acquire spatially ensembling features $\mathbf{x}^{l=3}$.

Experimental settings. As we directly implement our method from the official code of [67], we provide the values for HAT and GPM reported in [67]. For Omniglot Rotation and Split CIFAR-100 Superclass, we deploy the proposed architecture in multi-head settings with hyperparameters as reported in [93]. All our experiments run on a single-GPU setup of NVIDIA V100.

Performance metrics. We evaluate all methods based on the following four metrics:

- 1) **Accuracy (ACC)** measures the average of the final classification accuracy on all tasks: $\text{ACC} = \frac{1}{T} \sum_{i=1}^T A_{T,i}$, where $A_{T,i}$ is the test accuracy for task i after training on task T .
- 2) **Backward Transfer (BWT)** measures the forgetting during continual learning. Negative BWT means

that learning new tasks causes the forgetting of past tasks:

$$\text{BWT} = \frac{1}{T-1} \sum_{i=1}^{T-1} A_{T,i} - A_{i,i}.$$

Baselines. We compare our WSN with strong CL baselines; regularization-based methods: HAT [70] and EWC [37], rehearsal-based methods: GPM [67], and a pruning-based method: PackNet [53] and SupSup [89]. PackNet and SupSup is set to the baseline to show the effectiveness of re-used weights. We also compare with a naive sequential training strategy, referred to as FINETUNE. Multitask Learning (MTL) and Single-task Learning (STL) are not a CL method. MTL trains on multiple tasks simultaneously, and STL trains on single tasks independently.

4.2 Video incremental Learning (VIL)

We validate our method on video benchmark datasets against continual learning baselines on Video Incremental Learning (VIL). We consider continual video representation learning with a multi-head configuration (session id, i.e., s is given in training and inference) for all experiments in the paper. We follow the experimental setups in NeRV [10] and HNeRV [9]. **Datasets and architectures.** We conducted an extended experiment on the UVG of 8/17 video sessions. The category index and order in UVG8 (1.bunny, 2.beauty, 3.bosphorus, 4.bee, 5.jockey, 6.setgo, 7.shake, 8.yacht) and UVG17 (1.bunny, 2.city, 3.beauty, 4.focus, 5.bosphorus, 6.kids, 7.bee, 8.pan, 9.jockey, 10.lips, 11.setgo, 12.race, 13.shake, 14.river, 15.yacht, 16.sunbath, 17.twilight). We employ NeRV as our baseline architecture and follow its details for a fair comparison. After the positional encoding, we apply 2 sparse MLP layers on the output of the positional encoding layer, followed by five sparse NeRV blocks with upscale factors of 5, 2, 2, 2, 2. These sparse NeRV blocks decode 1280×720 frames from the 16×9 feature map obtained after the sparse MLP layers. For the upscaling method in the sparse NeRV blocks, we also adopt PixelShuffle [72]. Fourier Subneural Operator (FSO) is used at the NeRV2 or NeRV3 layer, denoted as f -NeRV2 and f -NeRV3³. The positional encoding for the video index s and frame index t is as follows:

$$\begin{aligned} \Gamma(s, t) = [& \sin(b^0 \pi s), \cos(b^0 \pi s), \dots, \sin(b^{l-1} \pi s), \cos(b^{l-1} \pi s), \\ & \sin(b^0 \pi t), \cos(b^0 \pi t), \dots, \sin(b^{l-1} \pi t), \cos(b^{l-1} \pi t)], \end{aligned} \quad (11)$$

where the hyperparameters are set to $b = 1.25$ and $l = 80$ such that $\Gamma(s, t) \in \mathbb{R}^{1 \times 160}$. As differences from the previous NeRV model, the first layer of the MLP has its input size expanded from 80 to 160 to incorporate both frame and video indices, and distinct head layers after the NeRV block are utilized for each video. For the loss objective in Equation 8, α is set to 0.7. We evaluate the video quality, average video session quality, and backward transfer with two metrics: PSNR.

Baselines. To show the effectiveness, we compare our WSN+FSO with strong CL baselines: Single-Task Learning (STL), which trains on single tasks independently, EWC [37], which is a regularized baseline, iCaRL [64], and ESMER [68] which are current strong rehearsal-based baseline, WSN [33]

which is a current strong architecture-based baseline, and Multi-Task Learning (MTL) which trains on multiple video sessions simultaneously, showing the upper-bound of WSN. Except for STL, all models are trained and evaluated on multi-head settings where a video session and time (s, t) indices are provided.

Training. In all experiments, we follow the same experimental settings as NeRV [9] and HNeRV [9] for fair comparisons. We train WSN+FSO, NeRV (STL), and MTL using Adam optimizer with a learning rate $5e-4$. For the ablation study on UVG17, we use a cosine annealing learning rate schedule [50], batch size of 1, training epochs of 150, and warmup epochs of 30 unless otherwise denoted.

VIL's performance metrics of PSNR We evaluate all methods based on the following continual learning metrics:

- 1) *Average PSNR* measures the average of the final performances on all video sessions: $\text{PSNR} = \frac{1}{N} \sum_{s=1}^N A_{N,s}$, where $A_{N,s}$ is the test PSNR for session s after training on the final video session S .
- 2) *Backward Transfer (BWT) of PSNR* measures the video representation forgetting during continual learning. Negative BWT means that learning new video sessions causes the video representation forgetting of past sessions: $\text{BWT} = \frac{1}{N-1} \sum_{s=1}^{N-1} A_{N,s} - A_{s,s}$.

4.3 Few-shot Class Incremental Learning (FSCIL)

We introduce experimental setups - Few-Shot Class Incremental Learning (FSCIL) settings to provide soft-subnetworks' effectiveness. We empirically evaluate and compare our soft subnetworks with state-of-the-art methods and vanilla subnetworks in the following subsections.

Datasets. To validate the effectiveness of the soft subnetwork, we follow the standard FSCIL experimental setting. We randomly selected 60 classes as the base and 40 as new classes for CIFAR-100 and miniImageNet. In each incremental learning session, we construct 5-way 5-shot tasks by randomly picking five classes and sampling five training examples for each class; we set the first 100 classes of CUB-200-2011 as base classes and the remaining 100 classes as new categories split into 10 novel sessions (i.e., a 10-way 5-shot).

Baselines. We mainly compare our SoftNet [34] with architecture-based methods for FSCIL: FSLL [54] that selects important parameters for each session, and HardNet, representing a binary subnetwork. Furthermore, we compare other FSCIL methods such as iCaRL [64], Rebalance [30], TOPIC [81], IDLVQ-C [11], and F2M [71]. Fourier Subneural Operator (FSO) is used at the 3th residual blocks of ResNet18. The 3th residual block's output $x^{l=3}$ is merged into the $l = 4$ th residual block through the FSO to acquire spatially ensembling features $x^{l=4}$. We also include a joint training method [71] that uses all previously seen data, including the base and the following few-shot tasks for training as a reference. Furthermore, we fix the classifier re-training method (cRT) [32] for long-tailed classification trained with all encountered data as the approximated upper bound.

Experimental settings. The experiments are conducted with NVIDIA GPU RTX8000 on CUDA 11.0. We also randomly split each dataset into multiple sessions. We run each algorithm ten times for each dataset and report their mean

3. The f -NeRV3 code is available at <https://github.com/ihayong/PFNR.git>

accuracy. We adopt ResNet18 [27] as the backbone network. For data augmentation, we use standard random crop and horizontal flips. In the base session training stage, we select top- $c\%$ weights at each layer and acquire the optimal soft-subnetworks with the best validation accuracy. In each incremental few-shot learning session, the total number of training epochs is 6, and the learning rate is 0.02. We train new class session samples using a few minor weights of the soft-subnetwork (Conv4x layer of ResNet18) obtained by the base session learning.

5 RESULTS OF TASK-INCREMENTAL LEARNING

5.1 Comparisons with baselines in TIL

We use a multi-head setting to evaluate our WSN algorithm under the more challenging visual classification benchmarks. The WSN+FSO’s performances are compared with others in terms of two measurements on three major benchmark datasets as shown in Table 1. Our WSN+FSO outperformed all state-of-the-art, achieving the best average accuracy of 79.00%, 61.70%, and 72.04%. WSN+FSO is also a forget-free model (BWT = ZERO), aligned with architecture-based models such as PackNet, SupSup, and WSN in these experiments. In addition, to show the effectiveness of the large single-scale task performance, we prepare WSN+FSO trained on the ImageNet-1K dataset, as shown in Table 9. WSN+FSO outperformed all baselines.

5.2 Statistics of WSN+FSO’s Representations in TIL

In the TinyImageNet task, the TinyImageNet takes 4 convolutional operators, followed by 3 fully connected layers. These operations represent more abstract features pooled by high-frequency components while losing low-frequency ones. To compensate for low-frequency components, we add an FSO to CNN architecture as shown in Figure 4. The lower layer’s output $x^{l=2}$ is merged into the $l = 3$ th layer residual block through the FSO to acquire spatially ensembling features $x^{l=3}$. The FSO also provides additional parameters to push the residual to zero. We will show the differences between ensembling features (WSN+FSO) and single features (WSN) represented by residual blocks as shown in Figure 5: WSN+FSO provides lower variances of feature maps and higher frequency components than WSN. The ensemble of representations led to better performances in TIL.

6 RESULTS OF VIDEO INCREMENTAL LEARNING

6.1 Comparisons with Baselines

Peak signal-to-noise ratio (PSNR). To compare WSN+FSO with conventional representative continual learning methods such as EWC, iCaRL, ESMER, and WSN+FSO, we prepare the reproduced results, as shown in Table 2. The architecture-based WSN outperformed the regularized method and replay method. The sparseness of WSN does not significantly affect sequential video representation results on two sequential benchmark datasets. Our WSN+FSO outperforms all conventional baselines including WSN and MLT (upper-bound of WSN) on the UVG17 benchmark datasets. Moreover, our performances of WSN with f -NeRV3 are better than those

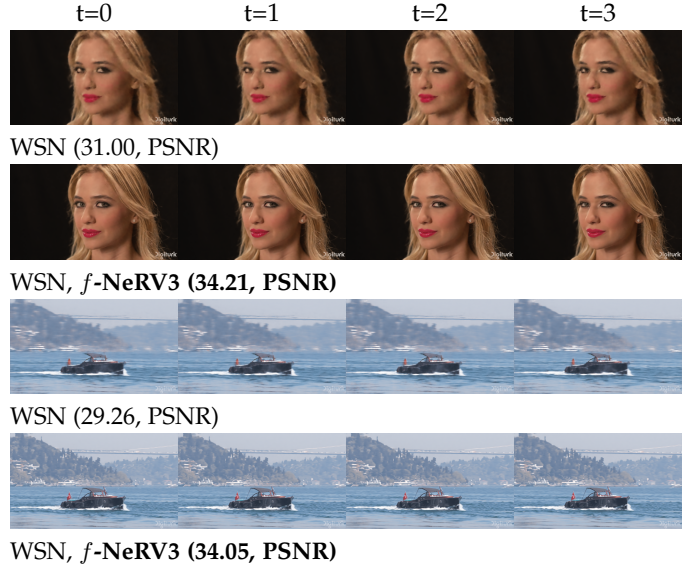


Fig. 6: **Video Generation** (from $t=0$ to $t=3$) with $c = 30.0\%$ on the UVG17 dataset.

of f -NeRV2 since f -NeRV3 tends to represent local textures, stated in the following Section 6.2. Note that the number of parameters of MLT is precisely the same as those of WSN.

Compression. We follow NeRV’s video quantization and compression pipeline [10], except for the model pruning step, to evaluate performance drops and backward transfer in the video sequential learning, as shown in Figure 10. Once sequential training is done, our WSN+FSO doesn’t need any extra pruning and finetuning steps, unlike NeRV. This point is our key advantage of WSN+FSO over NeRV. Figure 10 (a) shows the results of various sparsity and bit-quantization on the UVG17 datasets: the 8bit WSN+FSO’s performances are comparable with 32bit ones without a significant video quality drop. From our observations, the 8-bit subnetwork seems to be enough for video implicit representation. Figure 10 (b) shows the rate-distortion curves. We compare WSN+FSO with WSN and NeRV (STL). For a fair comparison, we take steps of pruning, fine-tuning, quantizing, and encoding NeRV. Our WSN+FSO outperforms all baselines.

Performance and Capacity. Our WSN+FSO outperforms WSN and MTL, as stated in Figure 11 (a). This result might suggest that properly selected weights in Fourier space lead to generalization more than others in VIL. Moreover, to show the behavior of FSO, We prepare a progressive WSN+FSO’s capacity and investigate how FSO reuses weights over sequential video sessions, as shown in Figure 11 (b). WSN+FSO tends to progressively transfer weights used for a prior session to weights for new ones, but the proportion of reused weights gets smaller as video sessions increase.

6.2 WSN+FSO’s Video Representations

We prepare the results of video generation as shown in Figure 6. We demonstrate that a sparse solution (WSN with $c = 30.0\%$, f -NeRV3) generates video representations sequentially without significant performance drops. Compared with WSN, WSN+FSO provides more precise representations. To find out the results, we inspect the layer-wise representations as shown in Figure 7, which offers

TABLE 1: Performance comparisons of the proposed method and other state-of-the-art including baselines - PackNet [53] and SupSup [89] - on various benchmark datasets. We report the mean and standard deviation of the average accuracy (ACC) and average backward transfer (BWT) across 5 independent runs with five seeds under the same experimental setup [17]. The best results are highlighted in bold. Also, \dagger denotes results reported from [17].

Method	CIFAR-100 Split		CIFAR-100 Superclass		TinyImageNet	
	ACC (%)	BWT (%)	ACC (%)	BWT (%)	ACC (%)	BWT (%)
La-MaML [22]	71.37 (± 0.7) \dagger	-5.39 (± 0.5) \dagger	54.44 (± 1.4) \dagger	-6.65 (± 0.9) \dagger	66.90 (± 1.7) \dagger	-9.13 (± 0.9) \dagger
GPM [67]	73.18 (± 0.5) \dagger	-1.17 (± 0.3) \dagger	57.33 (± 0.4) \dagger	-0.37 (± 0.1) \dagger	67.39 (± 0.5) \dagger	1.45 (± 0.2)\dagger
FS-DGPM [17]	74.33 (± 0.3) \dagger	-2.71 (± 0.2) \dagger	58.81 (± 0.3) \dagger	-2.97 (± 0.4) \dagger	70.41 (± 1.3) \dagger	-2.11 (± 0.9) \dagger
PackNet [53]	72.39 (± 0.4)	0.0	58.78 (± 0.5)	0.0	55.46 (± 1.2)	0.0
SupSup [89]	75.47 (± 0.3)	0.0	61.70 (± 0.3)	0.0	59.60 (± 1.1)	0.0
WSN*, $c = 50.0\%$	77.67 (± 0.1)	0.0	61.58 (± 0.0)	0.0	69.88 (± 1.7)	0.0
WSN, $c = 50.0\%$ + FSO	79.00 (± 0.3)	0.0	61.70 (± 0.2)	0.0	72.04 (± 0.7)	0.0
Multitask	79.75 (± 0.4) \dagger	-	61.00 (± 0.2) \dagger	-	77.10 (± 1.1) \dagger	-

TABLE 2: PSNR results with Fourier Subnueral Operator (FSO) layer (f -NeRV*) on UVG17 Video Sessions with average PSNR and Backward Transfer (BWT) of PSNR. Note that * denotes our reproduced results.

Method	Video Sessions																	Avg. MS-SSIM BWT
	1	2	3	4	5	6	7	8	9	10	11	12	13	14	15	16	17	
STL, NeRV [9]	39.63	-	36.06	-	37.35	-	41.23	-	38.14	-	31.86	-	37.22	-	32.45	-	-	- / -
STL, NeRV*	39.66	44.89	36.28	41.13	38.14	31.53	42.03	34.74	36.58	36.85	29.22	31.81	37.27	34.18	31.45	38.41	43.86	36.94 / -
EWC [37]*	11.15	9.21	12.71	11.40	15.58	9.25	7.06	12.96	6.34	10.31	9.55	13.39	5.76	8.67	10.93	10.92	28.29	11.38 / -16.13
iCaRL [64]*	24.31	28.25	22.19	22.74	22.84	16.55	29.37	17.92	16.65	27.43	13.64	16.42	24.02	21.60	19.40	18.60	26.46	21.67 / -6.23
ESMER [68]*	30.77	26.33	22.79	21.35	23.76	13.64	28.25	15.22	16.71	23.78	13.35	15.23	18.21	19.22	24.59	20.61	22.42	20.95 / -15.23
WSN*, $c = 30.0\%$	31.50	34.37	31.00	32.38	29.26	23.08	31.96	22.64	22.07	33.48	18.34	20.45	27.21	24.33	23.09	21.23	29.13	26.80 / 0.0
WSN*, $c = 50.0\%$	34.02	34.93	31.04	31.74	28.95	23.07	31.26	22.32	21.93	33.35	18.22	20.34	26.88	24.22	22.72	21.30	28.86	26.77 / 0.0
WSN, $c = 30.0\%$ + f -NeRV2	32.01	35.84	32.97	35.17	31.24	24.82	36.01	25.85	24.83	35.76	20.50	22.79	30.40	27.37	25.52	25.40	32.70	29.36 / 0.0
WSN, $c = 30.0\%$ + f -NeRV3	33.64	39.24	34.21	37.79	34.05	27.17	38.17	29.79	26.56	36.18	22.97	24.36	32.50	30.22	27.62	29.15	35.68	31.72 / 0.0
MLT (upper-bound)	32.39	34.35	31.45	34.03	30.70	24.53	37.13	27.83	23.80	34.69	20.77	22.37	32.71	28.00	25.89	26.40	33.16	29.42 / -

essential observations that WSN+FSO tends to capture local textures broadly at the NeRV3 layer while WSN focuses on local objects. This WSN+FSO behavior could lead to more generalized performances. Moreover, we conduct an ablation study to inspect the sparsity-wise performances of f -NeRV3 while holding the remaining parameters' sparsity ($c=50.0\%$), as shown in Figure 8. We could observe that as the sparsity of f -NeRV3 increases, its performances drop. This leads us to the importance of f -NeRV3's representations.

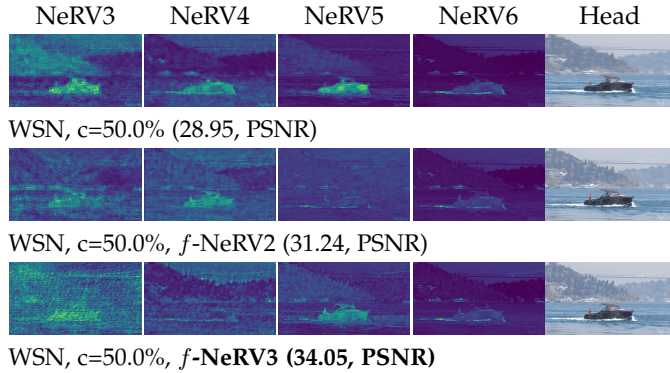


Fig. 7: WSN's Representations of NeRV Blocks with $c = 50.0\%$ on the UVG17 dataset.

6.3 Statistics of WSN+FSO's Representations in ViL

We provide the statistics of WSN+FSO's video representations, as shown in Figure 9. In the video incremental task, the NeRV architecture takes stems of 2 fully connected layers, followed by 5 convolutional operators. These operations represent an image up-scaled by multiple scalars while losing high-frequency representations (see WSN's representations of Figure 7). To compensate for high-frequency components,

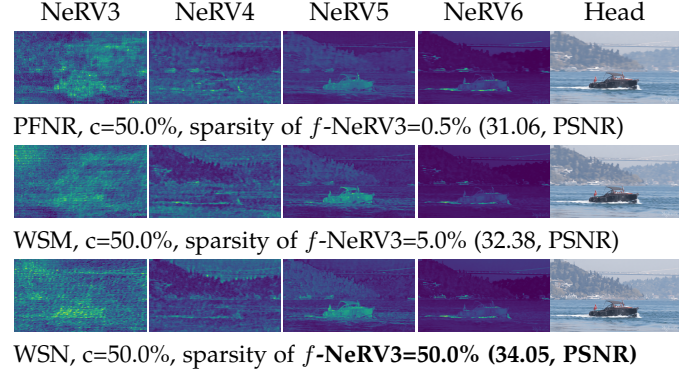


Fig. 8: Various sparsity of f -NeRV3 ranging from 0.05 % (top row) to 50.0 % (bottom row) on the UVG17 dataset.

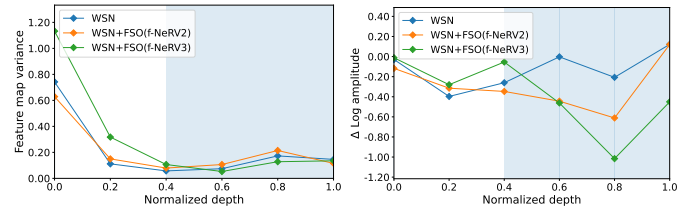


Fig. 9: The comparisons of WSN of NeRV Blocks (blue area) with FSO (white area) in terms of Feature variances and high-frequency components: the (a) offers the variance of the feature map and the (b) provides $\Delta \log$ amplitudes at high-frequency (1.0π).

we add an FSO to NeRV blocks as shown in Figure 3. The Conv. layer's output is merged into the outputs of FSO to acquire spatially ensembling features. We will show the differences between ensembling features (WSN+FSO) and single features (WSN), as shown in Figure 9: WSN+FSO provides a high variance of representations and higher

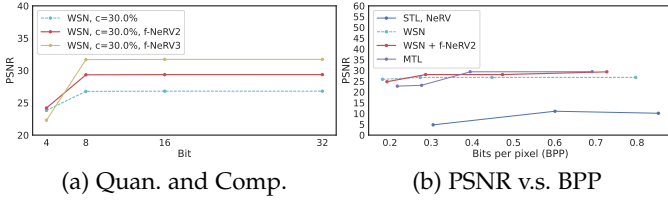
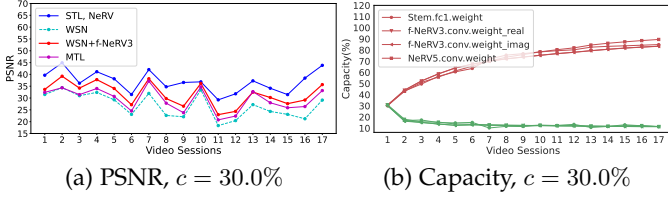


Fig. 10: PSNR v.s. Bits-per-pixel (BPP) on the UVG17 datasets.

Fig. 11: WSN+FSO's Comparison of PSNR with others and layer-wise accumulated capacities on the UVG17 dataset. Note that, in (b), green represents the percentage of reused subnetwork's parameters of Stem, f -NeRV3, and NeRV5 at the current session (s) obtained at the past ($s-1$) video sessions

frequency components than WSN at NeRV block 3. The ensemble of representations led to better performances in VIL, supporting the representations of Figure 7.

6.4 Ablation Studies of WSN+FSO

Variations of FSO. We prepared several ablation studies to prove the effectiveness of FSO. First, we show the performances of only real part (ignore an imaginary part) in f -NeRV2/3 as shown in Table 3. The PSNR performances of only real part were lower than those of both real and imaginary parts in f -NeRV2/3. We infer that the imaginary part of the winning ticket improves the implicit neural representations. Second, we also investigate the effectiveness of only FSO without Conv. Layer in f -NeRV2/3, as shown in Table 4. The PSNR performances were lower than FSO with Conv block. Therefore, the ensemble of FSO and Conv improves the implicit representations. Lastly, we investigate the effectiveness of sparse FSO in STL, as shown in Table 5. The sparse FSO boots the PSNR performances in STL. These ablation studies further strengthen the effectiveness of FSO for sequential neural implicit representations.

TABLE 3: WSN+Fourier Subnueral Operator (FSO) layer (f -NeRV*, $c=50.0\%$) on UVG8 Video Sessions with average PSNR and Backward Transfer (BWT). Note that *w/o imag.* ignores the imaginary part in f -NeRV*.

Method	Video Sessions								Avg. PSNR / BWT
	1	2	3	4	5	6	7	8	
f -NeRV2	34.46	33.91	32.17	36.43	25.26	20.74	30.18	25.45	29.82 / 0.0
f -NeRV2 <i>w/o imag.</i>	34.34	33.79	32.04	36.40	25.11	20.59	30.17	25.27	29.71 / 0.0
f -NeRV3	36.45	35.15	35.10	38.57	28.07	23.06	32.83	27.70	32.12 / 0.0
f -NeRV3 <i>w/o imag.</i>	35.66	34.65	34.09	37.95	25.80	21.94	32.17	26.91	31.15 / 0.0

TABLE 4: WSN+Fourier Subnueral Operator (FSO) layer (f -NeRV*, $c=50.0\%$) on UVG8 Video Sessions with average PSNR and Backward Transfer (BWT). Note that *w/o conv.* ignores the conv. layer in f -NeRV*.

Method	Video Sessions								Avg. PSNR / BWT
	1	2	3	4	5	6	7	8	
f -NeRV2	34.46	33.91	32.17	36.43	25.26	20.74	30.18	25.45	29.82 / 0.0
f -NeRV2 <i>w/o conv.</i>	30.05	32.10	30.12	31.82	24.00	19.60	28.21	24.47	27.54 / 0.0
f -NeRV3	36.45	35.15	35.10	38.57	28.07	23.06	32.83	27.70	32.12 / 0.0
f -NeRV3 <i>w/o conv.</i>	35.46	35.06	34.98	38.23	28.00	22.98	32.57	27.45	31.84 / 0.0

TABLE 5: WSN+Fourier Subnueral Operator (FSO) layer (f -NeRV*) on UVG8 Video Sessions with average PSNR and Backward Transfer (BWT).

Method	Video Sessions								Avg. PSNR / BWT
	1	2	3	4	5	6	7	8	
STL, NeRV [10]*	39.66	36.28	38.14	42.03	36.58	29.22	37.27	31.45	36.33 / -
STL, NeRV, f -NeRV2	39.73	36.30	38.29	42.03	36.64	29.25	37.35	31.65	36.40 / -
STL, NeRV, f -NeRV3	42.75	37.65	42.05	42.36	40.01	34.21	40.15	36.15	39.41 / -

Forget-free Transfer Matrix. We prepare the transfer matrix to prove our WSN+FSO's forget-freeness and to show video correlation among other videos, as shown in Figure 12 on the UVG17 dataset; lower triangular estimated by each session subnetwork denotes that our WSN+FSO is a forget-free method and upper triangular calculated by current session subnetwork denotes the video similarity between source and target. The WSN+FSO proves the effectiveness from the lower triangular of Figure 12 (a) and (b). Nothing special is observable from the upper triangular since they are not correlated, however, there might be some shared representations.

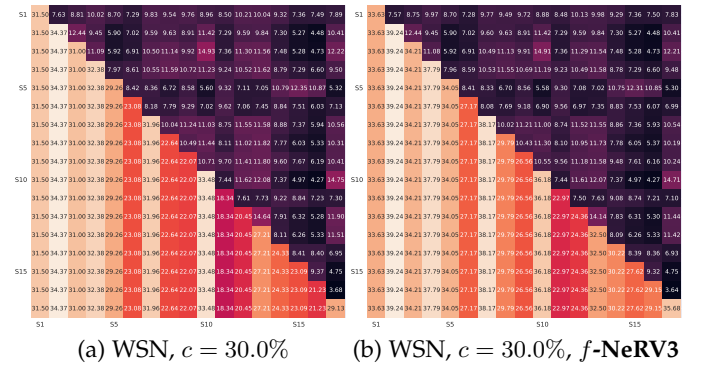


Fig. 12: Transfer Matrixes on the UVG17 dataset measured by PSNR of source and target videos.

7 RESULTS ON FEW-SHOT CIL (FSCIL)

7.1 Results and Comparisons

Comparisons with SOTA. We compare SoftNet+FSO with the following state-of-art-methods on TOPIC class split [81] of three benchmark datasets - CIFAR100 (Table 6), miniImageNet (Table 7), and CUB-200-2011 (Table 8). Leveraged by regularized backbone ResNet, SoftNet+FSO outperformed all existing architecture baselines FSLL [54], FACT [98], and WaRP [36] on CIFAR100, miniImageNet. On CUB-200-201, the performances of SoftNet+FSO are comparable with those of ALICE and LIMIT, considering that ALICE used class/data augmentations and LIMIT added an extra multi-head attention layer. Before finetuning SoftNet+FSO on CUB-200-201, we pre-trained WSN+FSO on the ImageNet-1K dataset, as shown in Table 9. The WSN+FSO outperforms WSN and baselines.

8 CONCLUSION

Inspired by *Regularized Lottery Ticket Hypothesis (RLTH)*, which states that competitive subnetworks exist within a dense network in continual learning tasks, we introduce an interpretable continual learning approach referred to as *Winning Subnetworks*, WSN, which leverages re-used weights within dense networks in Task Incremental Learning (TIL)

TABLE 6: Classification accuracy of ResNet18 on CIFAR-100 for 5-way 5-shot incremental learning with the same class split as in TOPIC [14]. * denotes the results reported from [71]. † represents our reproduced results.

Method	sessions									The gap with cRT
	1	2	3	4	5	6	7	8	9	
cRT [71]*	72.28	69.58	65.16	61.41	58.83	55.87	53.28	51.38	49.51	
TOPIC [14]	64.10	55.88	47.07	45.16	40.11	36.38	33.96	31.55	29.37	-20.14
CEC [97]	73.07	68.88	65.26	61.19	58.09	55.57	53.22	51.34	49.14	-0.37
F2M [71]	71.45	68.10	64.43	60.80	57.76	55.26	53.53	51.57	49.35	-0.16
LIMIT [99]	73.81	72.09	67.87	63.89	60.70	57.77	55.67	53.52	51.23	+1.72
MetaFSCIL [15]	74.50	70.10	66.84	62.77	59.48	56.52	54.36	52.56	49.97	+0.46
ALICE [62]	79.00	70.50	67.10	63.40	61.20	59.20	58.10	56.30	54.10	+4.59
Entropy-Reg [49]	74.40	70.20	66.54	62.51	59.71	56.58	54.52	52.39	50.14	+0.63
C-FSCIL [28]	77.50	72.45	67.94	63.80	60.24	57.34	54.61	52.41	50.23	+0.72
FSLL [54]	64.10	55.85	51.71	48.59	45.34	43.25	41.52	39.81	38.16	-11.35
FACT [98]	74.60	72.09	67.56	63.52	61.38	58.36	56.28	54.24	52.10	+2.59
WaRP [36]	80.31	75.86	71.87	67.58	64.39	61.34	59.15	57.10	54.74	+5.23
SoftNet, $c = 90\%$	79.97	75.75	71.76	67.36	64.09	60.91	59.07	56.94	54.76	+5.25
SoftNet, $c = 90\% + \text{FSO}$	80.40	76.06	72.43	68.43	65.54	62.27	60.13	58.15	56.00	+6.49

TABLE 7: Classification accuracy of ResNet18 on miniImageNet for 5-way 5-shot incremental learning with the same class split as in TOPIC [14]. * denotes results reported from [71].

Method	sessions									The gap with cRT
	1	2	3	4	5	6	7	8	9	
cRT [71]*	72.08	68.15	63.06	61.12	56.57	54.47	51.81	49.86	48.31	-
TOPIC [14]	61.31	50.09	45.17	41.16	37.48	35.52	32.19	29.46	24.42	-23.89
IDLQ-C [11]	64.77	59.87	55.93	52.62	49.88	47.55	44.83	43.14	41.84	-6.47
CEC [97]	72.00	66.83	62.97	59.43	56.70	53.73	51.19	49.24	47.63	-0.68
F2M [71]	72.05	67.47	63.16	59.70	56.71	53.77	51.11	49.21	47.84	-0.43
LIMIT [99]	73.81	72.09	67.87	63.89	60.70	57.77	55.67	53.52	51.23	+2.92
MetaFSCIL [15]	72.04	67.94	63.77	60.29	57.58	55.16	52.90	50.79	49.19	+0.88
ALICE [62]	80.60	70.60	67.40	64.50	62.50	60.00	57.80	56.80	55.70	+7.39
C-FSCIL [28]	76.40	71.14	66.46	63.29	60.42	57.46	54.78	53.11	51.41	+3.10
Entropy-Reg [49]	71.84	67.12	63.21	59.77	57.01	53.95	51.55	49.52	48.21	-0.10
Subspace Reg. [1]	80.37	71.69	66.94	62.53	58.90	55.00	51.94	49.76	46.79	-1.52
FSLL [54]	66.48	61.75	58.16	54.16	51.10	48.53	46.54	44.20	42.28	-6.03
FACT [98]	72.56	69.63	66.38	62.77	60.60	57.33	54.34	52.16	50.49	+2.18
WaRP [36]	72.99	68.10	64.31	61.30	58.64	56.08	53.40	51.72	50.65	+2.34
SoftNet, $c = 85\%$	79.50	74.54	70.29	66.39	63.35	60.38	57.32	55.22	53.92	+5.61
SoftNet, $c = 85\% + \text{FSO}$	79.72	74.72	70.73	66.88	64.05	61.82	58.03	56.01	54.80	+6.49

TABLE 8: Classification accuracy of ResNet18 on CUB-200-2011 for 10-way 5-shot incremental learning (TOPIC class split [81]). * denotes results reported from [71]. † represents our reproduced results.

Method	sessions											The gap with cRT
	1	2	3	4	5	6	7	8	9	10	11	
cRT [71]*	77.16	74.41	71.31	68.08	65.57	63.08	62.44	61.29	60.12	59.85	59.30	-
TOPIC [14]	68.68	62.49	54.81	49.99	45.25	41.40	38.35	35.36	32.22	28.31	26.28	-34.80
SPPR [100]	68.68	61.85	57.43	52.68	50.19	46.88	44.65	43.07	40.17	39.63	37.33	-21.97
CEC [97]	75.85	71.94	68.50	63.50	62.43	58.27	57.73	55.81	54.83	53.52	52.28	-7.02
F2M [71]	77.13	73.92	70.27	66.37	64.34	61.69	60.52	59.38	57.15	56.94	55.89	-3.41
LIMIT [99]	75.89	73.55	71.99	68.14	67.42	63.61	62.40	61.35	59.91	58.66	57.41	-1.89
MetaFSCIL [15]	75.90	72.41	68.78	64.78	62.96	59.99	58.30	56.85	54.78	53.82	52.64	-6.66
ALICE [62]	77.40	72.70	70.60	67.20	65.90	63.40	62.90	61.90	60.50	60.60	60.10	-0.02
Entropy-Reg [49]	75.90	72.14	68.64	63.76	62.58	59.11	57.82	55.89	54.92	53.58	52.39	-6.91
FSLL [54]	72.77	69.33	65.51	62.66	61.10	58.65	57.78	57.26	55.59	55.39	54.21	-6.87
FACT [98]	75.90	73.23	70.84	66.13	65.56	62.15	61.74	59.83	58.41	57.89	56.94	-2.36
WaRP [36]	77.74	74.15	70.82	66.90	65.01	62.64	61.40	59.86	57.95	57.77	57.01	-2.29
SoftNet, $c = 90\%$	78.07	74.58	71.37	67.54	65.37	62.60	61.07	59.37	57.53	57.21	56.75	-2.55
SoftNet, $c = 90\% + \text{FSO}$	78.24	74.73	71.37	67.54	65.54	62.80	61.92	59.54	57.86	57.72	56.84	-2.46

TABLE 9: Image Classification Performances on ImageNet-1K.

Method	Acc@1	Acc@5
ResNet18 [26]	69.75	89.07
WSN, $c=99.0\%$	69.46	89.05
WSN, $c=99.0\% + \text{FSO}$	70.63	89.84

scenarios. We have also introduced variants of WSN, such as Soft-subnetwork (SoftNet), to address the overfitting in few-shot class incremental learning (FSCIL). Additionally, To overcome the limitation of WSN (sparse re-used weights) in video incremental learning (VIL), we have a newly proposed module as another variant of WSN that aims to find an adaptive and compact sub-module referred to as *Fourier*

Subneural Operator (FSO) in Fourier space to encode videos in each video training session. The FSO finds reusable winning subnetworks in Fourier space, providing various bandwidths. We extend Fourier representations to various continual learning scenarios such as VIL, TIL, and FSCIL. Extensive experiments demonstrate the effectiveness of FSO in three continual learning scenarios. Overall, FSO’s representation markedly enhanced task performance at different convolutional representational levels, the higher layers for TIL and FSCIL and the lower layers for VIL.

Acknowledgement. This work was supported by Institute for Information & communications Technology Promotion (IITP) grant funded by No. 2021-0-01381 and 2022-0-00184.

REFERENCES

- [1] Afra Feyza Akyürek, Ekin Akyürek, Derry Wijaya, and Jacob Andreas. Subspace regularizers for few-shot class incremental learning. *arXiv preprint arXiv:2110.07059*, 2021.
- [2] Rahaf Aljundi, Eugene Belilovsky, Tinne Tuytelaars, Laurent Charlin, Massimo Caccia, Min Lin, and Lucas Page-Caccia. Online continual learning with maximal interfered retrieval. In *Advances in Neural Information Processing Systems (NeurIPS)*, 2019.
- [3] Yoshua Bengio, Nicholas Léonard, and Aaron C. Courville. Estimating or propagating gradients through stochastic neurons for conditional computation. *CoRR*, 2013.
- [4] Arslan Chaudhry, Naeemullah Khan, Puneet K Dokania, and Philip HS Torr. Continual learning in low-rank orthogonal subspaces. In *Advances in Neural Information Processing Systems (NeurIPS)*, 2020.
- [5] Arslan Chaudhry, Marc’Aurelio Ranzato, Marcus Rohrbach, and Mohamed Elhoseiny. Efficient lifelong learning with a-gem. In *Proceedings of the International Conference on Learning Representations (ICLR)*, 2019.
- [6] Arslan Chaudhry, Marcus Rohrbach, Mohamed Elhoseiny, Thalaiyasingam Ajanthan, Puneet K Dokania, Philip HS Torr, and M Ranzato. Continual learning with tiny episodic memories. *arXiv preprint arXiv:1902.10486*, 2019.
- [7] Geng Chen, Wendong Zhang, Han Lu, Siyu Gao, Yunbo Wang, Mingsheng Long, and Xiaokang Yang. Continual predictive learning from videos. In *Proceedings of the IEEE/CVF Conference on Computer Vision and Pattern Recognition*, pages 10728–10737, 2022.
- [8] Hao Chen, Matt Gwilliam, Bo He, Ser-Nam Lim, and Abhinav Shrivastava. Cnerv: Content-adaptive neural representation for visual data. *arXiv preprint arXiv:2211.10421*, 2022.
- [9] Hao Chen, Matt Gwilliam, Ser-Nam Lim, and Abhinav Shrivastava. Hnerv: A hybrid neural representation for videos. *arXiv preprint arXiv:2304.02633*, 2023.
- [10] Hao Chen, Bo He, Hanyu Wang, Yixuan Ren, Ser Nam Lim, and Abhinav Shrivastava. Nerv: Neural representations for videos. *Advances in Neural Information Processing Systems*, 34:21557–21568, 2021.
- [11] Kuilin Chen and Chi-Guhn Lee. Incremental few-shot learning via vector quantization in deep embedded space. In *International Conference on Learning Representations*, 2020.
- [12] Tianlong Chen, Zhenyu Zhang, Sijia Liu, Shiyu Chang, and Zhangyang Wang. Long live the lottery: The existence of winning tickets in lifelong learning. In *Proceedings of the International Conference on Learning Representations (ICLR)*, 2021.
- [13] Zhiqin Chen and Hao Zhang. Learning implicit fields for generative shape modeling. In *Proceedings of the IEEE/CVF Conference on Computer Vision and Pattern Recognition*, pages 5939–5948, 2019.
- [14] Ali Cheraghian, Shafin Rahman, Pengfei Fang, Soumava Kumar Roy, Lars Petersson, and Mehrtash Harandi. Semantic-aware knowledge distillation for few-shot class-incremental learning. In *Proceedings of the IEEE/CVF Conference on Computer Vision and Pattern Recognition*, pages 2534–2543, 2021.
- [15] Zhixiang Chi, Li Gu, Huan Liu, Yang Wang, Yuanhao Yu, and Jin Tang. Metafscl: A meta-learning approach for few-shot class incremental learning. In *Proceedings of the IEEE/CVF Conference on Computer Vision and Pattern Recognition*, pages 14166–14175, 2022.
- [16] Junwoo Cho, Seungtae Nam, Daniel Rho, Jong Hwan Ko, and Eunbyung Park. Streamable neural fields. In *European Conference on Computer Vision*, pages 595–612. Springer, 2022.
- [17] Danruo Deng, Guangyong Chen, Jianye Hao, Qiong Wang, and Pheng-Ann Heng. Flattening sharpness for dynamic gradient projection memory benefits continual learning. In *Advances in Neural Information Processing Systems (NeurIPS)*, 2021.
- [18] Misha Denil, Babak Shakibi, Laurent Dinh, Marc Aurelio Ranzato, and Nando de Freitas. Predicting parameters in deep learning. In *Advances in Neural Information Processing Systems (NeurIPS)*, 2013.
- [19] Arthur Douillard, Alexandre Ramé, Guillaume Couairon, and Matthieu Cord. Dytox: Transformers for continual learning with dynamic token expansion. In *Proceedings of the IEEE/CVF Conference on Computer Vision and Pattern Recognition*, pages 9285–9295, 2022.
- [20] Jonathan Frankle and Michael Carbin. The lottery ticket hypothesis: Finding sparse, trainable neural networks. In *Proceedings of the International Conference on Learning Representations (ICLR)*, 2019.
- [21] Siavash Golkar, Michael Kagan, and Kyunghyun Cho. Continual learning via neural pruning. *arXiv preprint arXiv:1903.04476*, 2019.
- [22] Gunshi Gupta, Karmesh Yadav, and Liam Paull. La-maml: Look-ahead meta learning for continual learning. In *Advances in Neural Information Processing Systems (NeurIPS)*, 2020.
- [23] Song Han, Jeff Pool, John Tran, and William Dally. Learning both weights and connections for efficient neural network. In *Proceedings of the International Conference on Learning Representations (ICLR)*, 2016.
- [24] Demis Hassabis, Dharshan Kumaran, Christopher Summerfield, and Matthew Botvinick. Neuroscience-inspired artificial intelligence. *Neuron*, 95(2):245–258, 2017.
- [25] Bo He, Xitong Yang, Hanyu Wang, Zuxuan Wu, Hao Chen, Shuaiyi Huang, Yixuan Ren, Ser-Nam Lim, and Abhinav Shrivastava. Towards scalable neural representation for diverse videos. *arXiv preprint arXiv:2303.14124*, 2023.
- [26] Kaiming He, Xiangyu Zhang, Shaoqing Ren, and Jian Sun. Deep residual learning for image recognition, 2015.
- [27] Kaiming He, Xiangyu Zhang, Shaoqing Ren, and Jian Sun. Deep residual learning for image recognition. In *Proceedings of the IEEE conference on computer vision and pattern recognition*, pages 770–778, 2016.
- [28] Michael Hersche, Geethan Karunaratne, Giovanni Cherubini, Luca Benini, Abu Sebastian, and Abbas Rahimi. Constrained few-shot class-incremental learning. In *Proceedings of the IEEE/CVF Conference on Computer Vision and Pattern Recognition*, pages 9057–9067, 2022.
- [29] Geoffrey Hinton. Neural networks for machine learning, 2012.
- [30] Saihui Hou, Xinyu Pan, Chen Change Loy, Zilei Wang, and Dahua Lin. Learning a unified classifier incrementally via rebalancing. In *Proceedings of the IEEE/CVF Conference on Computer Vision and Pattern Recognition*, pages 831–839, 2019.
- [31] Sangwon Jung, Hongjoon Ahn, Sungmin Cha, and Taesup Moon. Continual learning with node-importance based adaptive group sparse regularization. In *Advances in Neural Information Processing Systems (NeurIPS)*, 2020.
- [32] Bingyi Kang, Saining Xie, Marcus Rohrbach, Zhicheng Yan, Albert Gordo, Jiashi Feng, and Yannis Kalantidis. Decoupling representation and classifier for long-tailed recognition. *arXiv preprint arXiv:1910.09217*, 2019.
- [33] Haeyong Kang, Rusty John Lloyd Mina, Sultan Rizky Hikmawan Madjid, Jaehong Yoon, Mark Hasegawa-Johnson, Sung Ju Hwang, and Chang D Yoo. Forget-free continual learning with winning subnetworks. In *International Conference on Machine Learning*, pages 10734–10750. PMLR, 2022.
- [34] Haeyong Kang, Jaehong Yoon, Sultan Rizky Hikmawan Madjid, Sung Ju Hwang, and Chang D Yoo. On the soft-subnetwork for few-shot class incremental learning. *arXiv preprint arXiv:2209.07529*, 2022.
- [35] Muhammad Gul Zain Ali Khan, Muhammad Ferjad Naeem, Luc Van Gool, Didier Stricker, Federico Tombari, and Muhammad Zeshan Afzal. Introducing language guidance in prompt-based continual learning. In *Proceedings of the IEEE/CVF International Conference on Computer Vision*, pages 11463–11473, 2023.
- [36] Do-Yeon Kim, Dong-Jun Han, Jun Seo, and Jaekyun Moon. Warping the space: Weight space rotation for class-incremental few-shot learning. In *The Eleventh International Conference on Learning Representations*, 2023.
- [37] James Kirkpatrick, Razvan Pascanu, Neil Rabinowitz, Joel Veness, Guillaume Desjardins, Andrei A Rusu, Kieran Milan, John Quan, Tiago Ramalho, Agnieszka Grabska-Barwinska, Demis Hassabis, Claudia Clopath, Dharshan Kumaran, and Raia Hadsell. Overcoming catastrophic forgetting in neural networks. 2017.
- [38] Nikola Kovachki, Zongyi Li, Burigede Liu, Kamyar Azizzadenesheli, Kaushik Bhattacharya, Andrew Stuart, and Anima Anandkumar. Neural operator: Learning maps between function spaces. *arXiv preprint arXiv:2108.08481*, 2021.
- [39] Alex Krizhevsky, Geoffrey Hinton, et al. Learning multiple layers of features from tiny images. 2009.
- [40] Alex Krizhevsky, Ilya Sutskever, and Geoffrey E Hinton. Imagenet classification with deep convolutional neural networks. *Advances in neural information processing systems*, 25:1097–1105, 2012.
- [41] Abhishek Kumar and Hal Daume III. Learning task grouping and overlap in multi-task learning. In *Proceedings of the International Conference on Machine Learning (ICML)*, 2012.
- [42] Yann LeCun. The mnist database of handwritten digits. 1998.
- [43] Hao Li, Asim Kadav, Igor Durdanovic, Hanan Samet, and Hans Peter Graf. Pruning filters for efficient convnets. *arXiv preprint arXiv:1608.08710*, 2016.

- [44] Xilai Li, Yingbo Zhou, Tianfu Wu, Richard Socher, and Caiming Xiong. Learn to grow: A continual structure learning framework for overcoming catastrophic forgetting. In *Proceedings of the International Conference on Machine Learning (ICML)*, 2019.
- [45] Zhizhong Li and Derek Hoiem. Learning without forgetting. In *Proceedings of the European Conference on Computer Vision (ECCV)*, 2016.
- [46] Zizhang Li, Mengmeng Wang, Huaijin Pi, Kechun Xu, Jianbiao Mei, and Yong Liu. E-nerv: Expedite neural video representation with disentangled spatial-temporal context. In *Computer Vision—ECCV 2022: 17th European Conference, Tel Aviv, Israel, October 23–27, 2022, Proceedings, Part XXXV*, pages 267–284. Springer, 2022.
- [47] Zongyi Li, Nikola Kovachki, Kamyar Azizzadenesheli, Burigede Liu, Kaushik Bhattacharya, Andrew Stuart, and Anima Anandkumar. Fourier neural operator for parametric partial differential equations. *arXiv preprint arXiv:2010.08895*, 2020.
- [48] Zongyi Li, Nikola Kovachki, Kamyar Azizzadenesheli, Burigede Liu, Kaushik Bhattacharya, Andrew Stuart, and Anima Anandkumar. Neural operator: Graph kernel network for partial differential equations. *arXiv preprint arXiv:2003.03485*, 2020.
- [49] Huan Liu, Li Gu, Zhixiang Chi, Yang Wang, Yuanhao Yu, Jun Chen, and Jin Tang. Few-shot class-incremental learning via entropy-regularized data-free replay. *arXiv preprint arXiv:2207.11213*, 2022.
- [50] Ilya Loshchilov and Frank Hutter. Sgdr: Stochastic gradient descent with warm restarts. *arXiv preprint arXiv:1608.03983*, 2016.
- [51] Shishira R Maiya, Sharath Girish, Max Ehrlich, Hanyu Wang, Kwot Sin Lee, Patrick Poisson, Pengxiang Wu, Chen Wang, and Abhinav Shrivastava. Nirvana: Neural implicit representations of videos with adaptive networks and autoregressive patch-wise modeling. *arXiv preprint arXiv:2212.14593*, 2022.
- [52] Arun Mallya, Dillon Davis, and Svetlana Lazebnik. Piggyback: Adapting a single network to multiple tasks by learning to mask weights. In *Proceedings of the European Conference on Computer Vision (ECCV)*, 2018.
- [53] Arun Mallya and Svetlana Lazebnik. Packnet: Adding multiple tasks to a single network by iterative pruning. In *Proceedings of the IEEE conference on Computer Vision and Pattern Recognition*, pages 7765–7773, 2018.
- [54] Pratik Mazumder, Pravendra Singh, and Piyush Rai. Few-shot lifelong learning. *arXiv preprint arXiv:2103.00991*, 2021.
- [55] Michael McCloskey and Neal J Cohen. Catastrophic interference in connectionist networks: The sequential learning problem. In *Psychology of learning and motivation*, volume 24, pages 109–165. Elsevier, 1989.
- [56] Ishit Mehta, Michaël Gharbi, Connelly Barnes, Eli Shechtman, Ravi Ramamoorthi, and Manmohan Chandraker. Modulated periodic activations for generalizable local functional representations. In *Proceedings of the IEEE/CVF International Conference on Computer Vision*, pages 14214–14223, 2021.
- [57] Thomas Mensink, Jakob Verbeek, Florent Perronnin, and Gabriela Csurka. Distance-based image classification: Generalizing to new classes at near-zero cost. *IEEE transactions on pattern analysis and machine intelligence*, 35(11):2624–2637, 2013.
- [58] Ben Mildenhall, Pratul P Srinivasan, Matthew Tancik, Jonathan T Barron, Ravi Ramamoorthi, and Ren Ng. Nerf: Representing scenes as neural radiance fields for view synthesis. *Communications of the ACM*, 65(1):99–106, 2021.
- [59] Seyed Iman Mirzadeh, Mehrdad Farajtabar, Dilan Gorur, Razvan Pascanu, and Hassan Ghasemzadeh. Linear mode connectivity in multitask and continual learning. In *Proceedings of the International Conference on Learning Representations (ICLR)*, 2021.
- [60] Jeong Joon Park, Peter Florence, Julian Straub, Richard Newcombe, and Steven Lovegrove. Deepsdf: Learning continuous signed distance functions for shape representation. In *Proceedings of the IEEE/CVF conference on computer vision and pattern recognition*, pages 165–174, 2019.
- [61] Yixuan Pei, Zhiwu Qing, Shiwei Zhang, Xiang Wang, Yingya Zhang, Deli Zhao, and Xueming Qian. Space-time prompting for video class-incremental learning. In *Proceedings of the IEEE/CVF International Conference on Computer Vision (ICCV)*, pages 11932–11942, October 2023.
- [62] Can Peng, Kun Zhao, Tianren Wang, Meng Li, and Brian C Lovell. Few-shot class-incremental learning from an open-set perspective. In *European Conference on Computer Vision*, pages 382–397. Springer, 2022.
- [63] Vivek Ramanujan, Mitchell Wortsman, Aniruddha Kembhavi, Ali Farhadi, and Mohammad Rastegari. What’s hidden in a randomly weighted neural network? In *Proceedings of the IEEE International Conference on Computer Vision and Pattern Recognition (CVPR)*, 2020.
- [64] Sylvestre-Alvise Rebuffi, Alexander Kolesnikov, Georg Sperl, and Christoph H Lampert. icarl: Incremental classifier and representation learning. In *Proceedings of the IEEE conference on Computer Vision and Pattern Recognition*, pages 2001–2010, 2017.
- [65] Matthew Riemer, Ignacio Cases, Robert Ajemian, Miao Liu, Irina Rish, Yuhai Tu, and Gerald Tesauero. Learning to learn without forgetting by maximizing transfer and minimizing interference. *arXiv preprint arXiv:1810.11910*, 2018.
- [66] Andrei A Rusu, Neil C Rabinowitz, Guillaume Desjardins, Hubert Soyer, James Kirkpatrick, Koray Kavukcuoglu, Razvan Pascanu, and Raia Hadsell. Progressive neural networks. *arXiv preprint arXiv:1606.04671*, 2016.
- [67] Gobinda Saha, Isha Garg, and Kaushik Roy. Gradient projection memory for continual learning. In *Proceedings of the International Conference on Learning Representations (ICLR)*, 2021.
- [68] Fahad Sarfraz, Elahe Arani, and Bahram Zonooz. Error sensitivity modulation based experience replay: Mitigating abrupt representation drift in continual learning. In *The Eleventh International Conference on Learning Representations*, 2023.
- [69] Katja Schwarz, Yiyi Liao, Michael Niemeyer, and Andreas Geiger. Graf: Generative radiance fields for 3d-aware image synthesis. *Advances in Neural Information Processing Systems*, 33:20154–20166, 2020.
- [70] Joan Serra, Didac Suris, Marius Miron, and Alexandros Karatzoglou. Overcoming catastrophic forgetting with hard attention to the task. In *Proceedings of the International Conference on Machine Learning (ICML)*, 2018.
- [71] Guangyuan Shi, Jiaxin Chen, Wenlong Zhang, Li-Ming Zhan, and Xiao-Ming Wu. Overcoming catastrophic forgetting in incremental few-shot learning by finding flat minima. *Advances in Neural Information Processing Systems*, 34, 2021.
- [72] Wenzhe Shi, Jose Caballero, Ferenc Huszar, Johannes Totz, Andrew P Aitken, Rob Bishop, Daniel Rueckert, and Zehan Wang. Real-time single image and video super-resolution using an efficient sub-pixel convolutional neural network. In *Proceedings of the IEEE conference on computer vision and pattern recognition*, pages 1874–1883, 2016.
- [73] Hanul Shin, Jung Kwon Lee, Jaehon Kim, and Jiwon Kim. Continual learning with deep generative replay. In *Advances in Neural Information Processing Systems (NeurIPS)*, 2017.
- [74] Pravendra Singh, Vinay Kumar Verma, Pratik Mazumder, Lawrence Carin, and Piyush Rai. Calibrating cnns for lifelong learning. *Advances in Neural Information Processing Systems*, 33:15579–15590, 2020.
- [75] Vincent Sitzmann, Julien Martel, Alexander Bergman, David Lindell, and Gordon Wetzstein. Implicit neural representations with periodic activation functions. *Advances in Neural Information Processing Systems*, 33:7462–7473, 2020.
- [76] James Seale Smith, Paola Cascante-Bonilla, Assaf Arbelle, Donghyun Kim, Rameswar Panda, David Cox, Diyi Yang, Zsolt Kira, Rogerio Feris, and Leonid Karlinsky. Construct-vl: Data-free continual structured vl concepts learning. In *Proceedings of the IEEE/CVF Conference on Computer Vision and Pattern Recognition (CVPR)*, pages 14994–15004, June 2023.
- [77] James Seale Smith, Leonid Karlinsky, Vyshnavi Gutta, Paola Cascante-Bonilla, Donghyun Kim, Assaf Arbelle, Rameswar Panda, Rogerio Feris, and Zsolt Kira. Coda-prompt: Continual decomposed attention-based prompting for rehearsal-free continual learning. In *Proceedings of the IEEE/CVF Conference on Computer Vision and Pattern Recognition (CVPR)*, pages 11909–11919, June 2023.
- [78] Stanford. Available online at <http://cs231n.stanford.edu/tiny-imagenet-200.zip>. CS 231N, 2021.
- [79] Wenju Sun, Qingyong Li, Jing Zhang, Wen Wang, and Yangli-ao Geng. Decoupling learning and remembering: A bilevel memory framework with knowledge projection for task-incremental learning. In *Proceedings of the IEEE/CVF Conference on Computer Vision and Pattern Recognition*, pages 20186–20195, 2023.
- [80] Matthew Tancik, Pratul Srinivasan, Ben Mildenhall, Sara Fridovich-Keil, Nithin Raghavan, Utkarsh Singhal, Ravi Ramamoorthi, Jonathan Barron, and Ren Ng. Fourier features let networks learn high frequency functions in low dimensional domains. *Advances in Neural Information Processing Systems*, 33:7537–7547, 2020.

- [81] Xiaoyu Tao, Xiaopeng Hong, Xinyuan Chang, Songlin Dong, Xing Wei, and Yihong Gong. Few-shot class-incremental learning. In *Proceedings of the IEEE/CVF Conference on Computer Vision and Pattern Recognition*, pages 12183–12192, 2020.
- [82] Sebastian Thrun. *A Lifelong Learning Perspective for Mobile Robot Control*. Elsevier, 1995.
- [83] Michalis K Titsias, Jonathan Schwarz, Alexander G de G Matthews, Razvan Pascanu, and Yee Whye Teh. Functional regularisation for continual learning with gaussian processes. In *Proceedings of the International Conference on Learning Representations (ICLR)*, 2020.
- [84] Alasdair Tran, Alexander Mathews, Lexing Xie, and Cheng Soon Ong. Factorized fourier neural operators. *arXiv preprint arXiv:2111.13802*, 2021.
- [85] Andrés Villa, Juan León Alcázar, Motasem Alfarra, Kumail Alhamoud, Julio Hurtado, Fabian Caba Heilbron, Alvaro Soto, and Bernard Ghanem. Pivot: Prompting for video continual learning. *arXiv preprint arXiv:2212.04842*, 2022.
- [86] Yabin Wang, Zhiwu Huang, and Xiaopeng Hong. S-prompts learning with pre-trained transformers: An occam’s razor for domain incremental learning. *Advances in Neural Information Processing Systems*, 35:5682–5695, 2022.
- [87] Zifeng Wang, Zizhao Zhang, Sayna Ebrahimi, Ruoxi Sun, Han Zhang, Chen-Yu Lee, Xiaoqi Ren, Guolong Su, Vincent Perot, Jennifer Dy, et al. Dualprompt: Complementary prompting for rehearsal-free continual learning. In *European Conference on Computer Vision*, pages 631–648. Springer, 2022.
- [88] Zifeng Wang, Zizhao Zhang, Chen-Yu Lee, Han Zhang, Ruoxi Sun, Xiaoqi Ren, Guolong Su, Vincent Perot, Jennifer Dy, and Tomas Pfister. Learning to prompt for continual learning. In *Proceedings of the IEEE/CVF Conference on Computer Vision and Pattern Recognition*, pages 139–149, 2022.
- [89] Mitchell Wortsman, Vivek Ramanujan, Rosanne Liu, Aniruddha Kembhavi, Mohammad Rastegari, Jason Yosinski, and Ali Farhadi. Supermasks in superposition. In *Advances in Neural Information Processing Systems (NeurIPS)*, 2020.
- [90] Yue Wu, Yinpeng Chen, Lijuan Wang, Yuancheng Ye, Zicheng Liu, Yandong Guo, and Yun Fu. Large scale incremental learning. In *Proceedings of the IEEE/CVF Conference on Computer Vision and Pattern Recognition*, pages 374–382, 2019.
- [91] Ju Xu and Zhanxing Zhu. Reinforced continual learning. In *Advances in Neural Information Processing Systems (NeurIPS)*, 2018.
- [92] Shipeng Yan, Jiangwei Xie, and Xuming He. Der: Dynamically expandable representation for class incremental learning. In *Proceedings of the IEEE/CVF Conference on Computer Vision and Pattern Recognition*, pages 3014–3023, 2021.
- [93] Jaehong Yoon, Saehoon Kim, Eunho Yang, and Sung Ju Hwang. Scalable and order-robust continual learning with additive parameter decomposition. In *Proceedings of the International Conference on Learning Representations (ICLR)*, 2020.
- [94] Jaehong Yoon, Divyam Madaan, Eunho Yang, and Sung Ju Hwang. Online coreset selection for rehearsal-based continual learning. In *Proceedings of the International Conference on Learning Representations (ICLR)*, 2022.
- [95] Jaehong Yoon, Eunho Yang, Jeongtae Lee, and Sung Ju Hwang. Lifelong learning with dynamically expandable networks. In *Proceedings of the International Conference on Learning Representations (ICLR)*, 2018.
- [96] Friedemann Zenke, Ben Poole, and Surya Ganguli. Continual learning through synaptic intelligence. In *International Conference on Machine Learning*, pages 3987–3995. PMLR, 2017.
- [97] Chi Zhang, Nan Song, Guosheng Lin, Yun Zheng, Pan Pan, and Yinghui Xu. Few-shot incremental learning with continually evolved classifiers. In *Proceedings of the IEEE/CVF Conference on Computer Vision and Pattern Recognition*, pages 12455–12464, 2021.
- [98] Da-Wei Zhou, Fu-Yun Wang, Han-Jia Ye, Liang Ma, Shiliang Pu, and De-Chuan Zhan. Forward compatible few-shot class-incremental learning. In *Proceedings of the IEEE/CVF conference on computer vision and pattern recognition*, pages 9046–9056, 2022.
- [99] Da-Wei Zhou, Han-Jia Ye, Liang Ma, Di Xie, Shiliang Pu, and De-Chuan Zhan. Few-shot class-incremental learning by sampling multi-phase tasks. *IEEE Transactions on Pattern Analysis and Machine Intelligence*, 2022.
- [100] Kai Zhu, Yang Cao, Wei Zhai, Jie Cheng, and Zheng-Jun Zha. Self-promoted prototype refinement for few-shot class-incremental learning. In *Proceedings of the IEEE/CVF Conference on Computer Vision and Pattern Recognition*, pages 6801–6810, 2021.



Haeyong Kang (S'05) received the M.S. degree in Systems and Information Engineering from University of Tsukuba in 2007. From April 2007 to October 2010, he worked as an associate research engineer at LG Electronics. With working experiences at the Korea Institute of Science and Technology (KIST) and the University of Tokyo, He received a Ph.D. at the School of Electrical Engineering, the Korea Advanced Institute of Science and Technology (KAIST) with a dissertation on forget-free continual learning in 2023. He is pursuing research such as unbiased machine learning and continual learning as a postdoctoral researcher at KAIST.



with real-world data.

Jaehong Yoon He received the B.S. and M.S. degrees in Computer Science from Ulsan National Institute of Science and Technology (UNIST), and received the Ph.D. degree in the School of Computing from Korea Advanced Institute of Science and Technology (KAIST). He is currently working as a postdoctoral research associate at the University of North Carolina at Chapel Hill. His current research interests include multimodal learning, video understanding, efficient deep learning, continual learning, and learning



Sung Ju Hwang He received the B.S. degree in Computer Science and Engineering from Seoul National University. He received the M.S. and Ph.D. degrees in Computer Science from The University of Texas at Austin. From September 2013 to August 2014, he was a postdoctoral research associate at Disney Research. From September 2013 to December 2017, he was an assistant professor in the School of Electric and Computer Engineering at UNIST. Since 2017, he has been on the faculty at the Korea Advanced Institute of Science and Technology (KAIST), where he is currently a KAIST Endowed Chair Professor in the Kim Jaechul School of Artificial Intelligence and School of Computing at KAIST.



Chang D. Yoo (Senior Member, IEEE) He received the B.S. degree in Engineering and Applied Science from the California Institute of Technology, the M.S. degree in Electrical Engineering from Cornell University, and the Ph.D. degree in Electrical Engineering from the Massachusetts Institute of Technology. From January 1997 to March 1999, he was Senior Researcher at Korea Telecom (KT). Since 1999, he has been on the faculty at the Korea Advanced Institute of Science and Technology (KAIST), where he is currently a Full Professor with tenure in the School of Electrical Engineering and an Adjunct Professor in the Department of Computer Science. He also served as Dean of the Office of Special Projects and Dean of the Office of International Relations.